


RESEARCH

Open Access



Study on the Fracture Toughness of Polypropylene–Basalt Fiber-Reinforced Concrete

Ninghui Liang^{1,3*} , Lianxi Ren¹, Shuo Tian¹, Xinrong Liu¹, Zuliang Zhong¹, Zhiyun Deng^{2*} and Ru Yan¹

Abstract

To study the hybrid effects of polypropylene fiber and basalt fiber on the fracture toughness of concrete, 13 groups of notched concrete beam specimens with different fiber contents and mass ratios were prepared for the three-point bending test. Based on acoustic emission monitoring data, the initiation cracking load and instability load of each group of specimens were obtained, and the fracture toughness parameters were calculated according to the double-K fracture criterion. The test results show that the basalt fiber-reinforced concrete has a greater increase in initial fracture toughness, and the toughness of coarse polypropylene fiber-reinforced concrete is more unstable. Moreover, after the coarse polypropylene fiber content reaches 6 kg/m^3 and the basalt fiber content reaches 3 kg/m^3 , increasing the content will not significantly improve the fracture toughness of the concrete. The polypropylene–basalt fiber will produce positive and negative effects when mixed, and the mass ratio of 2:1 was optimal. Finally, the fitting analysis revealed that the fracture process of polypropylene–basalt fiber-reinforced concrete (PBFRC) can be objectively described by the bilinear softening constitutive curve improved by Xu and Reinhardt.

Keywords: hybrid-fiber concrete, three-point bending test, fracture toughness, fiber content, fiber mass ratio, bilinear softening curve

1 Introduction

With the emergence of large-span beams, super high-rise buildings and mass concrete structures, the requirements for concrete strength and ductility are increasing. Therefore, enhancing toughness and deformation performance have become an important problem to solve when the concrete strength increases, ductility decreases, and brittleness increases. It is one of the effective methods that adding fiber into concrete for improving the tensile

strength, crack toughness and impact resistance (Abdallah et al., 2016, 2017; Guler et al., 2019). Compared with plain concrete, fiber-reinforced concrete can improve the stiffness of the components, enhance the ductility and cracking resistance, and have good frost resistance under the same conditions (Das et al., 2018; Liang et al., 2019b; Mudadu et al., 2018). Besides, it has been widely used in high-rise buildings, underground engineering structure, marine engineering and bridge engineering.

Studies have shown that adding different fibers can improve the toughness of concrete in different manners. Steel fiber improves the strength of concrete, and enhances fracture load and toughness in the fracture process (Abdallah et al., 2016; Chi et al., 2014). However, steel fiber has defects, such as high cost, self-importance, easy to rust, and poor workability. To eliminate the disadvantage of steel fiber, other fibers should be considered to adopt to replace the steel fiber. Polypropylene fiber is

*Correspondence: liangninghui0705@163.com

² State Key Laboratory of Hydrosience and Engineering, Tsinghua University, 10084 Beijing, China

³ School of Civil Engineering, National Joint Engineering Research Center of Geohazards Prevention in the Reservoir Areas (Chongqing), and Key Laboratory of New Technology for Construction of Cities in Mountain Area (Chongqing University), Ministry of Education, Chongqing University, No. 83 Shabei Street, Shapingba District, 400045 Chongqing, China
Full list of author information is available at the end of the article
Journal information: ISSN 1976-0485 / eISSN 2234-1315

seen to possess some advantages compared to steel fiber: easy to work in concrete, better economy, light in weight, rarely corrode in concrete and resistant to aggressive chemicals (Deng et al. 2020b). Coarse polypropylene fiber (CF) has a larger size and a higher tensile strength of monofilament, which can inhibit the development of cracks in the later period, and is similar to steel fiber in terms of improving the durability and ductility of concrete (Buratti & Mazzotti, 2015; Buratti et al., 2011; Niu et al., 2018; Xia et al., 2013). Basalt fiber (BF) possesses excellent mechanical and physical properties, including high-temperature stability, superior tensile strength, good acid alkali-resistance, and excellent plastic deformation capacity, which is a new type of eco-friendly, cost-effective, high-performance, green and inorganic fiber (Branston et al., 2016; Jalsutram et al., 2017; Jiang et al., 2014; Wang et al., 2019). In addition, the basalt fiber has a small size and a large elastic modulus, which can inhibit the development of early micro cracks in the early stage.

Some researchers also believe that compared with the incorporation of single fiber, adding fibers with different elastic moduli, strengths and sizes into concrete can produce a positive hybrid effect in strengthening and toughening concrete, and more effectively improve the fracture toughness of concrete (Banthia et al., 2014; Kasagani & Rao, 2018; Wang et al., 2019). According to the previous researches, the fibers mixing ratio is the main factor affecting the mechanical properties (Abdallah et al., 2017; Liu, 2013), fracture parameters (Smarzewski, 2019; Soroushian et al., 1998) and flexural toughness (Smarzewski, 2018a, 2018b; Zhu et al., 2010) of concrete. In contrary, some results also show that polypropylene fibers and basalt fibers have no significant effect on the compressive strength (Ayub et al., 2014a, 2014b; Komlos et al., 1995) and flexural strength (Smarzewski, 2019) of concrete matrix.

Nowadays, the hybrid basalt–polypropylene fiber-reinforced concrete has been widely concerned by researches. These studies usually focused on the fresh, mechanical, and durability properties (Arslan, 2016; Ayub et al.,

2014a, 2014b; Jiang et al., 2016), impact-resistance behavior (Fu et al., 2018a, 2018b; Zhang et al., 2019), flexural toughness (Smarzewski, 2018a, 2018b) and fracture properties (Smarzewski, 2019, 2020) of hybrid basalt–polypropylene fiber-reinforced concrete. Besides, the polypropylene fibers used in their studies were fine fiber rather than the macro fiber. The coarse and long fibers determine the propagation of cracks and improve the toughness at the post-crack region (Afroughsabet & Ozbakkaloglu, 2015; Nataraja et al., 1999), while micro and short fibers bridge the micro-cracks thereby enhancing the peak strength (Betterman et al., 1995). To the author's knowledge, the scant work is available in the literature regarding the fracture toughness of concrete reinforced with the hybridization of micro basalt fiber and coarse polypropylene fiber.

In this paper, coarse polypropylene fiber and basalt fiber were selected for single blending and mixed blending in concrete. The effect of the two fibers on the fracture toughness of concrete was studied by the three-point bending test, acoustic emission technology and double-K fracture theory of concrete. The theoretical cohesive toughness of polypropylene–basalt fiber-reinforced concrete (PBFRC) specimens was obtained by calculating three double-line softening constitutive curves and comparing with the measured cohesive toughness. Then, a double-line softening constitutive curve suitable for hybrid fibers was obtained.

2 Experimental Program

2.1 Materials

The corrugated coarse polypropylene fiber (CF) was provided by Ningbo Dacheng New Material Co., Ltd, and the basalt fiber (BF) was provided by Beijing Tongshen Composite Material Co., Ltd, whose shapes and properties are shown in Fig. 1 and Table 1.

The cement was PO 52.5 grade ordinary Portland cement. The coarse aggregates were stones with grain sizes of 5–10 mm and 10–20 mm, and the fine aggregates

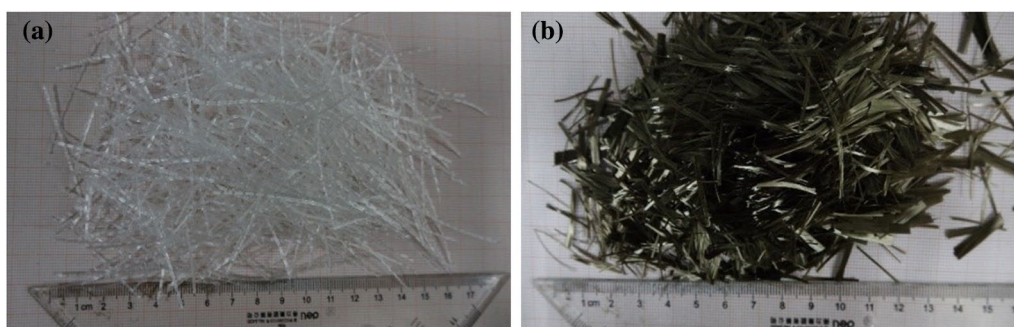
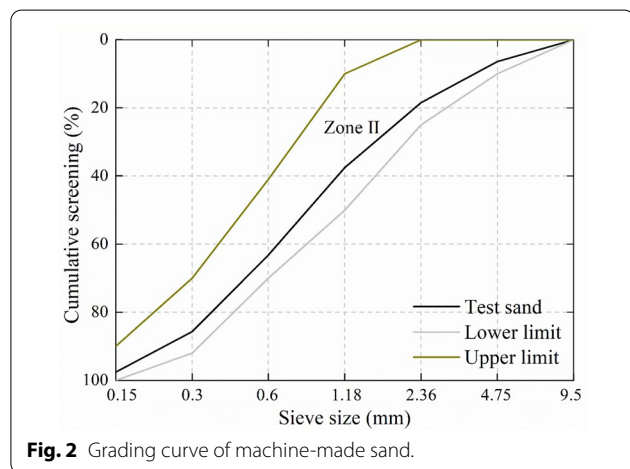


Fig. 1 External shapes of fibers: **a** CF; **b** BF.

Table 1 Properties of fibers.

Fiber type	Length (mm)	Diameter (mm)	Elastic modulus (GPa)	Density/(g/cm ³)	Tensile strength (MPa)
CF	50	0.8	7.4	0.95	706
BF	19	0.013	95–105	2.75	4000



were sands whose dimensions are less than 5 mm. As shown in Fig. 2, the fine aggregate met the requirements of Chinese standard JGJ-52 (JGJ-52 2006). Carboxylic acid superplasticizer was used, whose water reduction rate was 15–30%.

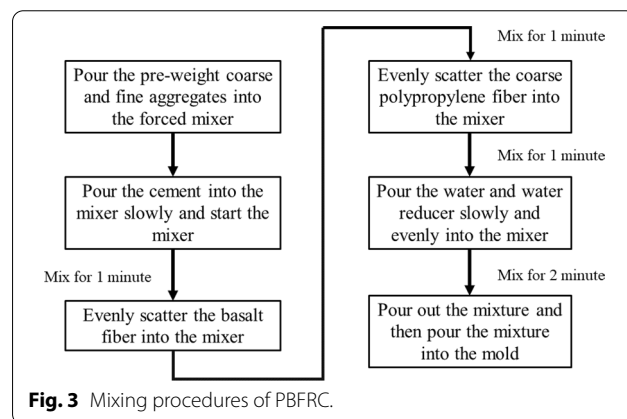
2.2 Preparation of Specimens

Except for the difference in fiber type and quantity, the mixing ratio of other materials in each group of specimens remained the same to reduce the performance difference of concrete samples due to the difference in raw material performance. The concrete strength grade is C50, and the ratio of cementitious materials is m (cement): m (water): m (sand): m (stone): m (water reducing agent) = 456: 164: 787: 1010: 4.56.

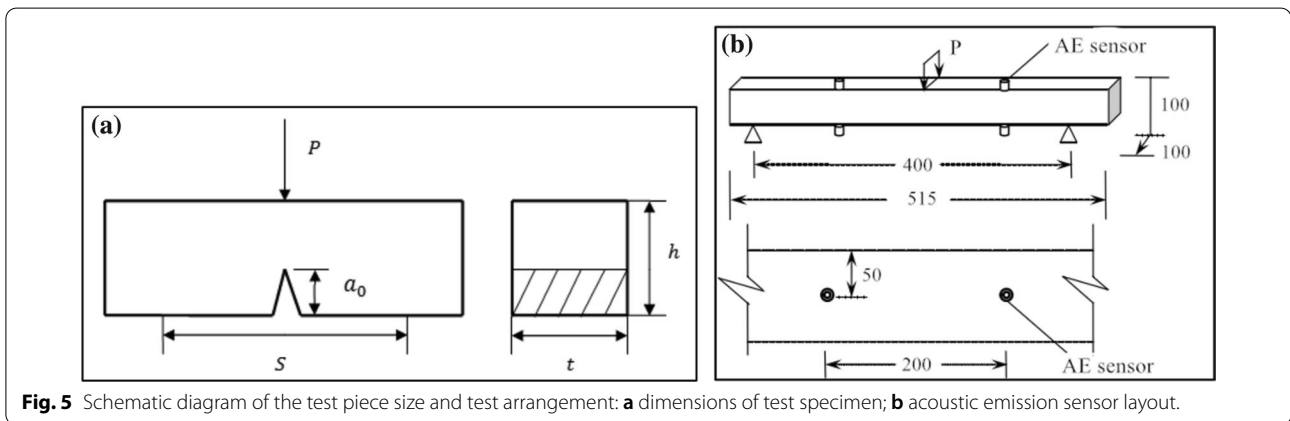
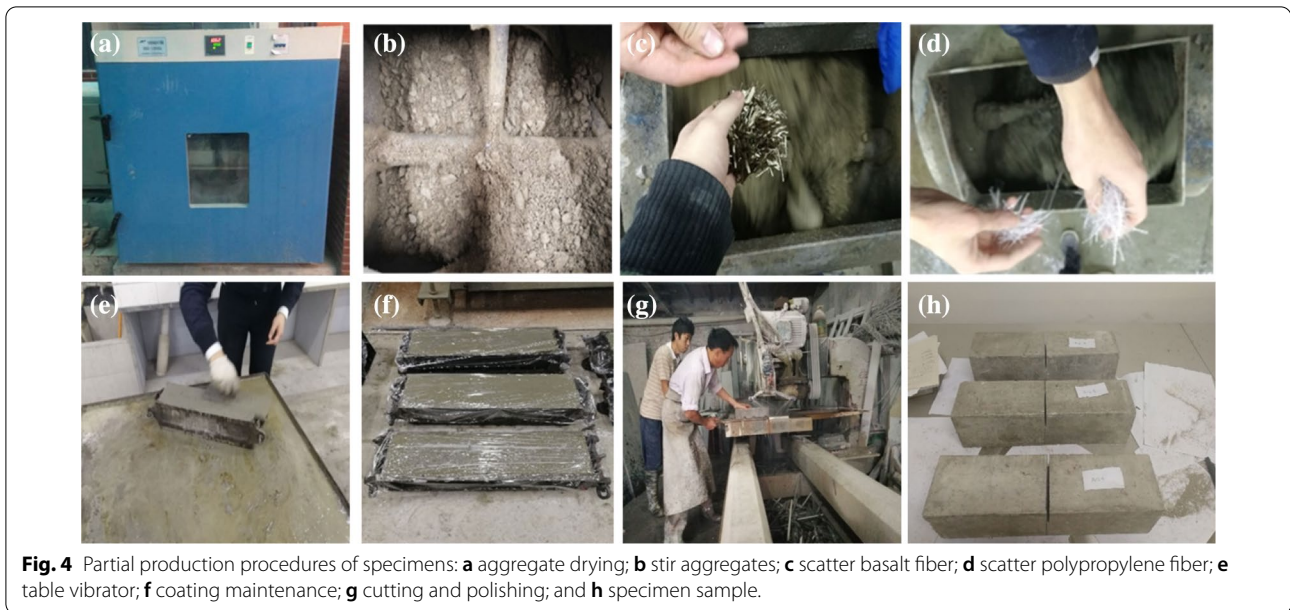
A total of 13 different fiber content were designed, including one control group (no fiber), two groups of CF, two groups of BF, as well as eight groups of hybrid polypropylene–basalt fiber with different fiber content. The coarse polypropylene fiber content was selected as 6 kg/m³ and 9 kg/m³, while the basalt fiber content was 3 kg/m³ and 6 kg/m³ according to previous experimental research and engineering experience (Banthia, 2005; Deng et al., 2020b; Liang et al. 2019c; Zieliński & Olszewski, 2005). Parameters of each group specimen for the three-point bending test are shown in Table 2. The fiber concrete mixing procedures are listed in Fig. 3.

Table 2 Parameters of each group of specimens.

Specimen	Fiber content (kg/m ³)		Compressive strength/MPa	Splitting tensile strength/MPa
	CF	BF		
A0	–	–	47.13	2.65
A1	6.0	–	49.01	3.15
A2	9.0	–	48.21	3.31
A3	–	3.0	49.06	2.68
A4	–	6.0	50.41	2.76
A5	4.8	1.2	50.93	3.21
A6	4.0	2.0	53.71	3.29
A7	3.0	3.0	53.24	3.02
A8	2.0	4.0	52.58	2.94
A9	1.2	4.8	51.32	2.84
A10	6.0	3.0	52.36	3.41
A11	4.5	4.5	51.25	3.24
A12	3.0	6.0	50.27	3.15



The mixing, pouring, curing and determination of related parameters of the test piece are carried out in accordance with Chinese standard CECS 13 (CECS-13 2009) and GB/T 50080 (GB/T-50080 2016). Partial production procedures of specimens are shown in Fig. 4. The test specimen shape is shown in Fig. 5a: the size was $L \times t \times h = 515 \text{ mm} \times 100 \text{ mm} \times 100 \text{ mm}$, the span length was $S = 400 \text{ mm}$, and the relative notch depth was $a_0/h = 0.4$. In addition, the curing age of all specimens when tested is 28 days. The acoustic emission instrument uses the SAEU2S-6 model acoustic emission collector and test system produced by Beijing Soft Island Times Technology Co., Ltd, which is mainly composed of sensors, amplifiers and acquisition boxes. Four acoustic emission probes were placed in the upper and lower center symmetrical positions of the left and right parts of the test piece, as shown in Fig. 5b.



2.3 Experimental Procedure

There were 13 groups of edge-notched simply supported concrete beams designed and fabricated with different fiber mixes for the three-point bending test according to Chinese standard DL/T5332 (DL/T5332-2005 2005). Three replicate specimens were conducted for each group.

The test apparatus is shown in Fig. 6. A CMT5504 microcomputer-controlled electronic universal testing machine was used for testing. The acoustic emission probes on the measured points were placed in advance and collected data while loading. The loading time and acoustic emission acquisition time were strictly controlled and synchronized to measure the cracking load and unstable load of the test specimen. The specimens were loaded with displacement control at a continuous



rate of 0.1 mm/min. The displacement of the crack opening was measured by a clamping extensometer. The gauge length of the extensometer was 12.5 mm, the range was 5 mm, and the accuracy was 0.001 mm.

During loading, the cracks were carefully observed and recorded to prevent sudden damage to the extensometer break. The load–displacement ($P-\delta$) curves were automatically generated by the testing machine system. In addition, the load–fracture opening-displacement ($P-CMOD$) curves were measured by the clip-in extensometer. Then, the initiation cracking load and instability load of concrete in the three-point bending test were compared with acoustic emission data.

3 Results and Discussion

3.1 Workability

The concrete used in the test belongs to dry hard concrete, its poor flow properties mixing was measured slump not greater than 10 mm. Based on Chinese standard GB/T-5008 (GB/T-50080 2016), its rheological characteristics were evaluated by the test of Vebe consistometer, and the test result is shown in Fig. 7.

Incorporating fiber makes the mixture of each group of PBFRC specimens become denser, which shows that the Vebe Consistency (VC) time becomes larger. Compared with the minimum content of coarse polypropylene fiber and basalt fiber which are 6 kg/m³ and 3 kg/m³, when the maximum content of polypropylene fiber and basalt fiber reaches 9 kg/m³ and 6 kg/m³, the VC time increased by 7.14% and 16.67%, respectively. Compared with A0, the VC time of A6–A8 with a total content of 6 kg/m³ increased by 8.70–13.04%, and A10–A12 with 9 kg/m³ increased by 21.74–26.09%. All show that increasing the amount of fiber will weaken the workability of the mixture. The cement paste in the matrix gradually adheres to the outer surface of the fibers, decreasing the

free-flowing cement paste, and finally deteriorating the flow performance of the PBFRC mixture (Fei et al., 2018).

For specimens A5–A9 with a total content of 6 kg/m³, when the mixing ratio of CF and BF was 4:1 and 2:1, respectively, the VC time increased by 17.39% and 13.04%. In addition, when the mixing ratio of was 1:4 and 1:2, both the VC time of concrete mixture increased by 8.70%. This indicated that the smaller the aspect ratio of the fiber, the greater the hindrance to the fluidity of the mixture. The coarse polypropylene fiber has a greater effect on the rheological properties of the concrete mixture than basalt fiber. The reason may be that the distribution density of polypropylene fibers is larger and can form a network structure in the PBFRC mixture, hinder the sinking of aggregates and inhibit the flow of free slurry. Therefore, the fibers are more difficult to distribute in concrete matrix due to the larger friction force, which may result in poor flow properties (Smarzewski and D’Aniello 2018).

3.2 Load–Displacement Curves

The load–displacement ($P-\delta$) curve and load–fracture opening-displacement ($P-CMOD$) curve of 13 sets of concrete specimens were obtained from the three-point bending test of the notched beam, as shown in Fig. 8. See Appendix 1 for raw data.

In Fig. 8, concrete specimen A0 experienced obvious brittle failure, and its bearing capacity dropped after the peak load and completely disappeared with the rapid failure of the specimen. The peak load and residual load of the specimens increased to varying degrees. The rising sections of the $P-\delta$ curve and $P-CMOD$ curve of the 3-kg/m³ specimen A3 and 6-kg/m³ specimen A4 with single-basalt fiber are basically consistent with those of specimen A0. After reaching the peak load, there was also a cliff-like decline, the load decreased to approximately 10% of the peak load, an inflection point appeared, and the curve began to gently decline until it returned to zero. The $P-\delta$ curve and $P-CMOD$ curve of the 6-kg/m³ specimen A1 and 9-kg/m³ specimen A2 with single-polypropylene fiber are basically consistent with those of specimen A0 in the rising section and falling section of the cliff, and the inflection point was approximately 20% peak load. Then, the load showed a slight and gentle growth trend with the increase in displacement until the displacement was 2.5 mm. Specimen A2 had a larger peak load than A1, and A3 had a lower peak load than A4, so the specimens with polypropylene fiber have advantages compared to those with the same content of basalt fiber in the peak load. Thus, in the optimal content range, a higher content of the same type of fiber corresponds to better performance of the concrete.

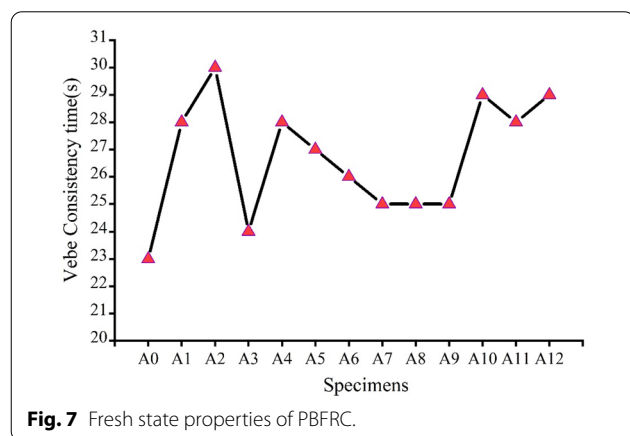
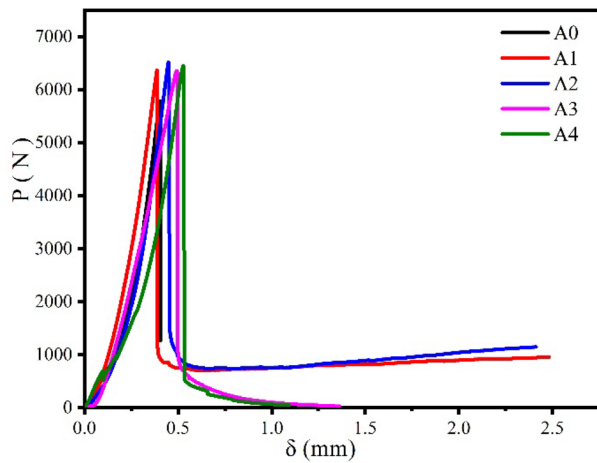
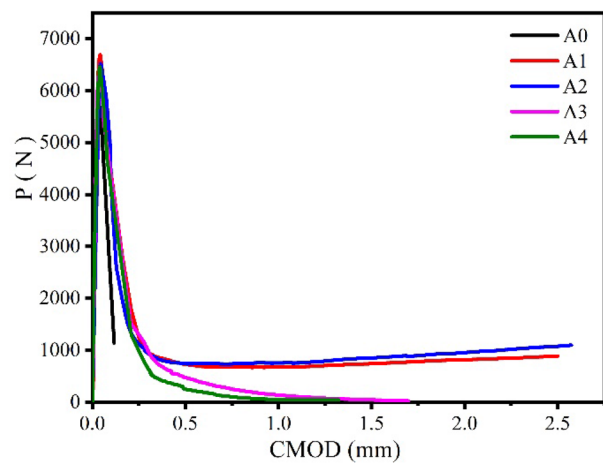


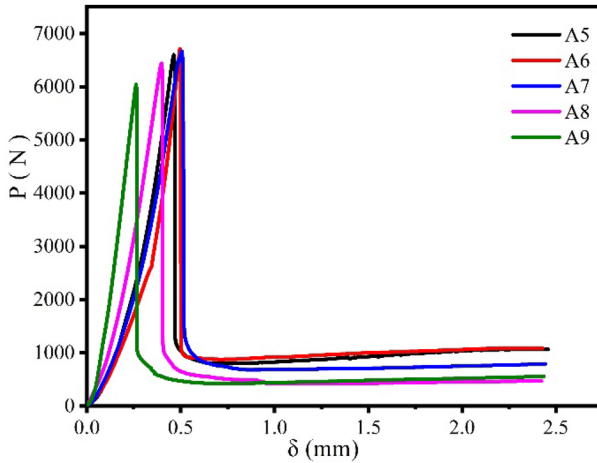
Fig. 7 Fresh state properties of PBFRC.



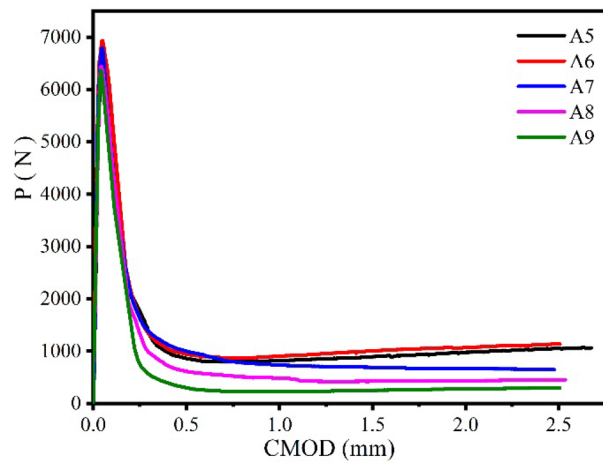
(a) Single doped $P-\delta$ curve



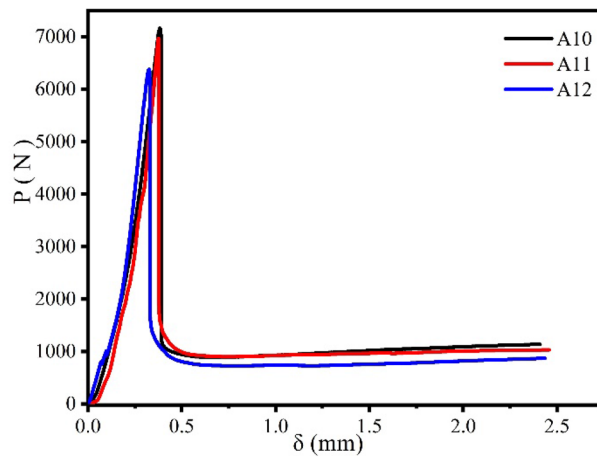
(b) Single doped $P-CMOD$ curve



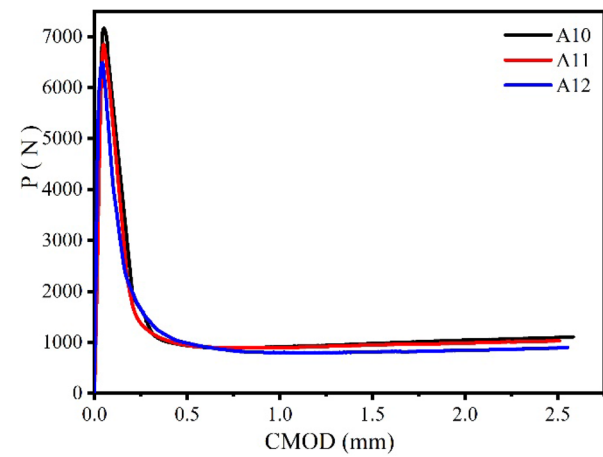
(c) $P-\delta$ curve of 6 kg/m^3



(d) $P-CMOD$ curve of 6 kg/m^3



(e) $P-\delta$ curve of 9 kg/m^3



(f) $P-CMOD$ curve of 9 kg/m^3

Fig. 8 Load-displacement curve and load-opening displacement curve.

Meanwhile, the concrete with polypropylene fiber exhibited better toughness than that with basalt fiber.

The P - δ curves and P - $CMOD$ curves of the 6-kg/m³ specimens A5–A9 and 9-kg/m³ specimens A10–A12 were similar to those of the sample of single-mixed polypropylene fiber. The peak load and residual load of the specimen generally first increased and subsequently decreased with the increase in the basalt content, which indicates that the mass ratio significantly affects the toughening effect of the hybrid-fiber-reinforced concrete.

3.3 Initiation Cracking Load and Instability Load

Concrete is a brittle material, and the crack development under load is divided into three stages: initiation, stable expansion and instability (Xu, 1999). Acoustic emission technology can accurately determine the cracking point and instability point of concrete, which reflect the internal damage of concrete. Figure 9 matches the time–load curve and time-cumulative ring count curve of specimen A1.

This method can effectively determine the initiation load and instability load of the concrete during the three-point bending test. The double-K fracture parameters of the specimens provide accurate data. The initiation cracking load (P_{ini}), instability load (P_c) and critical crack opening displacement ($CMOD_c$) of each group of test specimens are shown in Table 3. See Appendix 2 for relevant complete data.

In Table 3, compared with plain concrete specimen A0, the addition of polypropylene fiber and basalt fiber increased the initiation cracking load P_{ini} , instability load P_c and critical crack opening displacement $CMOD_c$. Compared with A0, specimen A1 of 6 kg/m³ and specimen A2 of 9 kg/m³ with single-polypropylene fiber had P_{ini} increased by 24.5% and 27.1%, P_c increased by 22.8% and 25.9%, and $CMOD_c$ increased by 19.4% and 24.7%.

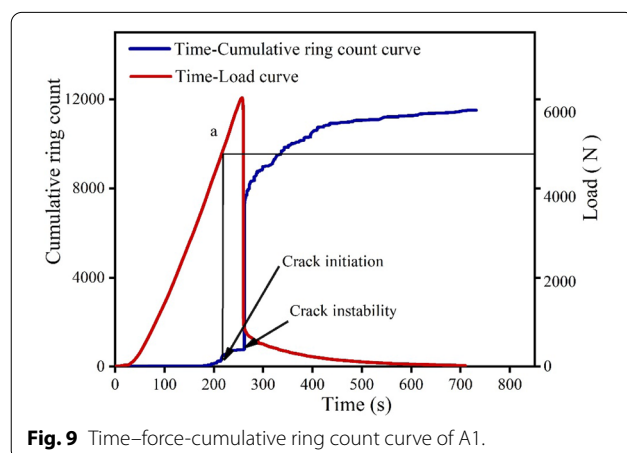


Fig. 9 Time–force–cumulative ring count curve of A1.

Table 3 The P_{ini} , P_c and $CMOD_c$ of each group specimen.

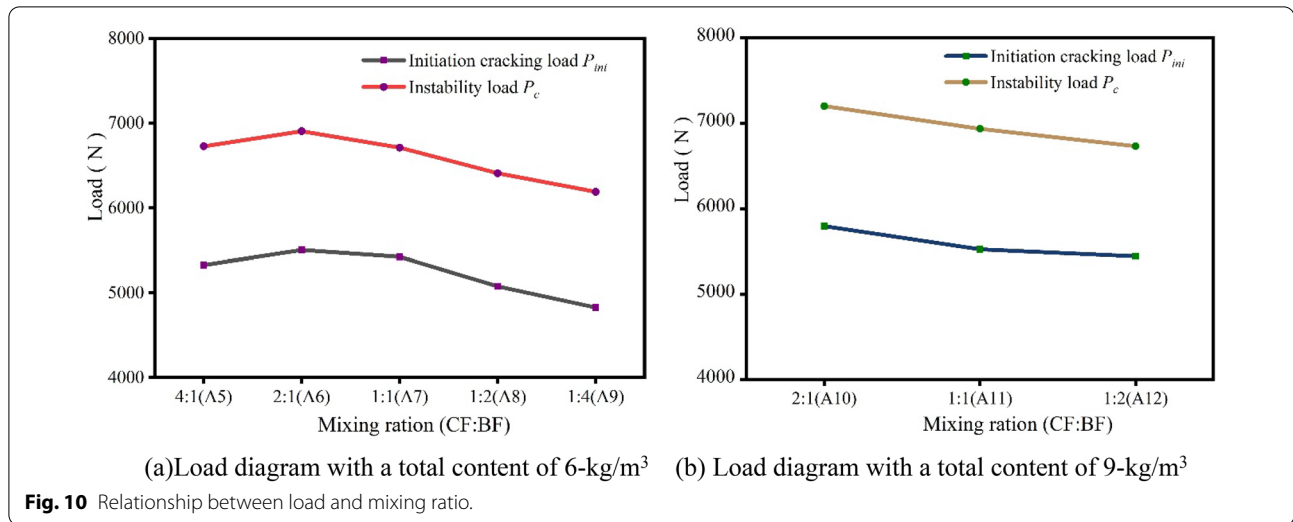
Specimen	Initiation cracking load P_{ini} (N)	Critical crack opening displacement $CMOD_c$ (mm)	Instability load P_c (N)
A0	4204	0.0372	5403
A1	5234	0.0444	6636
A2	5345	0.0464	6802
A3	4595	0.0410	6077
A4	4903	0.0416	6245
A5	5328	0.0461	6727
A6	5504	0.0487	6905
A7	5425	0.0457	6711
A8	5076	0.0426	6408
A9	4828	0.0402	6189
A10	5795	0.0508	7202
A11	5524	0.0491	6936
A12	5444	0.0459	6732

P_{ini} , P_c and $CMOD_c$ of specimen A3 with 3 kg/m³ of only basalt fiber increased by 9.3%, 12.5%, and 10.2%, respectively, and P_{ini} , P_c and $CMOD_c$ of specimen A4 with 6 kg/m³ increased by 16.6%, 15.6% and 11.8%, respectively. Thus, the incorporation of fiber improves the brittleness of concrete, and polypropylene fiber has a more significant effect than basalt fiber.

Compared with specimen A1, the P_{ini} and P_c of specimen A2 improved by 2.1% and 2.5%. Compared with specimen A4, the P_{ini} and P_c of specimen A3 increased by 6.7% and 2.8%. These two controls indicate that in the optimal content range, the polypropylene fiber content of 6–9 kg/m³ has little effect on the cracking load and fracture load of concrete, while the basalt fiber content of 3–6 kg/m³ significantly increases the cracking load of concrete.

Compared with A0, the P_{ini} , P_c and $CMOD_c$ of specimens A5–A9 with the total amount of 6 kg/m³ improved by 14.8–30.9%, 14.5–27.8% and 8.1–30.9%, respectively. P_{ini} , P_c and $CMOD_c$ of specimens A10–A12 with a total amount of 9 kg/m³ increased by 29.5–37.8%, 24.6–33.3% and 23.4–36.6%, respectively. Thus, the mixed-fiber-reinforced concretes with different contents and mass ratios presented different fracture performance indices, which indicates that the mixed-fiber specimen had better load-bearing performance than the single-fiber specimen under appropriate mixing conditions.

The load conditions of the hybrid-fiber-reinforced concrete specimens with different amounts and mass ratios are shown in Fig. 10. For specimens A5–A9 with a total content of 6 kg/m³, both initiation cracking load and fracture load first increased and subsequently decreased. The initiation load of 5504 N and instability load of

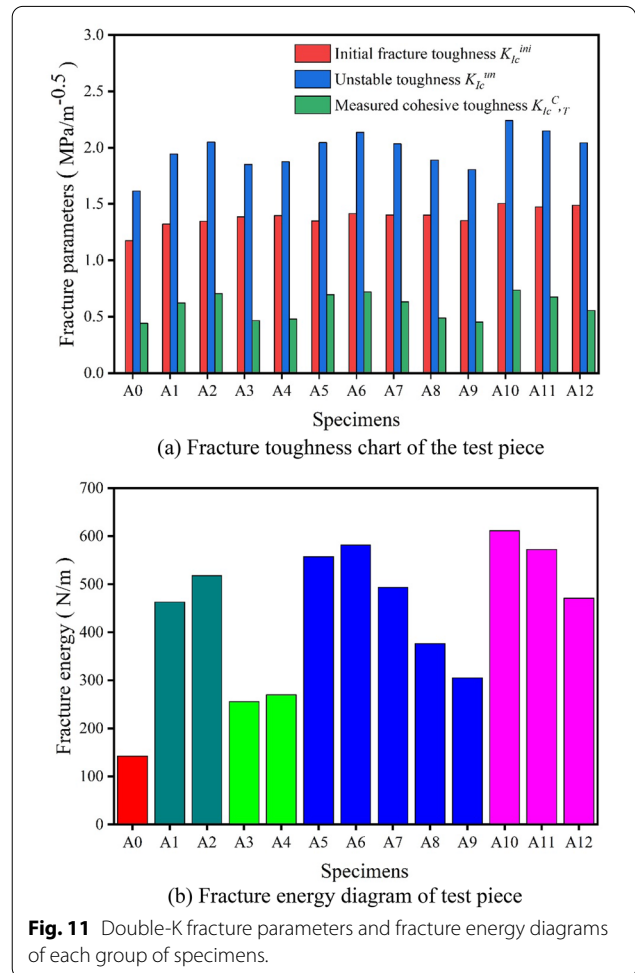


6905 N of specimen A6 are the maximum values of the same total content. For specimens A10–A12 with a total admixture of 9 kg/m³, both initiation load and instability load showed a decreasing trend. The initiation cracking load of 5795 N and instability load of 7202 N of specimen A10 are the maximum values of the same total content. Thus, the mixing effect of the 9-kg/m³ fiber concrete is stronger than that of 6 kg/m³. When the mixing ratio of CF and BF is 2:1, the initiation load and instability load of hybrid-fiber-reinforced concrete specimens most obviously improved.

3.4 Effect of Fiber on Double-K Fracture Parameters

The double-K fracture theory and simplified formula were proposed by Xu (1999), which well explained the fracture mechanism of concrete. The double-K fracture model believes that the fracture process of concrete is essentially the process of concrete’s own crack propagation under load. The process can be divided into three stages: the elastic stage when the crack does not propagate, the inelastic stage when the crack propagates steadily, and the instability stage when the crack propagates rapidly. By introducing the initiation toughness K_{Ic}^{ini} and instability toughness K_{Ic}^{un} to distinguish these three stages, that is the strength factor K of the crack tip of the concrete is compared with K_{Ic}^{ini} and K_{Ic}^{un} . When $K < K_{Ic}^{ini}$, the crack is in the elastic stage. When $K_{Ic}^{ini} < K < K_{Ic}^{un}$, the crack is in the inelastic stage. When $K > K_{Ic}^{un}$, crack is in the unstable stage. The toughness parameter has a relatively clear physical meaning and guiding significance for practical engineering and theoretical research.

The calculation steps of fracture parameters refer to other studies of this research team (Liang et al., 2019a,



2019c). In addition, the calculation results are shown in Fig. 11. See Appendix 3 for relevant complete data.

In Fig. 11a, the fracture toughness parameters K_{Ic}^{ini} , K_{Ic}^{un} , and $K_{Ic,T}^C$ of all fiber-added specimens increased compared to those of plain concrete specimen A0. As shown in Fig. 11b, the fracture energy of the fiber-added specimen is higher than that of the plain concrete specimen A0. Thus, both basalt fiber and polypropylene fiber can improve the fracture toughness parameters of concrete.

3.4.1 Single Doped Fiber Specimen

Compared specimen A1 of 6 kg/m³ with specimen A2 of 9 kg/m³ with coarse polypropylene fiber and specimen A3 of 3 kg/m³ with specimen A4 of 6 kg/m³ with basalt fiber. Each pair has relatively similar fracture toughness parameters, although the amount of the latter is increased by 3 kg/m³ compared to the former. Thus, after the fiber content reaches a certain amount, increasing the content cannot continue to significantly improve the fracture toughness of the concrete. Compared with plain concrete A0, fracture energy G_f of specimens A1 and A2 increased by 225.7% and 264.3%, which is a much higher increase than those of specimens A3 and A4 (increased by 58.9% and 89.9%), so polypropylene fiber has a greater effect on the fracture energy of concrete than basalt fiber.

Fiber blending can improve the fracture toughness parameters of concrete, which is mainly affected by its type and amount. Compared with plain concrete A0, initial fracture toughness K_{Ic}^{ini} of specimens A1 and A2 increased by 12.6% and 14.7%, while specimens A3 and A4 increased by 18.0% and 18.9%, which indicates that polypropylene fiber has a less obvious effect on the initial fracture toughness of concrete than basalt fiber. The reason is that the basalt fiber has a smaller diameter, which can reduce the initial defects of the concrete matrix and make the concrete matrix denser (Deng et al., 2020a). Basalt fiber in the concrete matrix can share the stress of part of the crack tip and delay the generation and development of micro cracks (Jiang et al., 2016). Polypropylene fiber has a larger diameter, which has limited effect on the stress concentration of the prefabricated crack tip of the concrete and little effect on the micro cracks (Liang et al., 2020). As a result, polypropylene fiber causes a relatively smaller increase in initial fracture toughness of concrete than basalt fiber.

Unstable toughness K_{Ic}^{un} of specimens A3 and A4 increased by only 15.2% and 16.1%, while those of specimens A1 and A2 significantly increased by 23.5% and 26.9%. Measured cohesive toughness $K_{Ic,T}^C$ of concrete reflects the magnitude of the load capacity that the specimen can withstand from cracking to instability. Compared to specimen A0, $K_{Ic,T}^C$ of specimens A3 and A4

increased by only 5.3% and 6.2%, while those of specimens A1 and A2 significantly increased by 49.0% and 56.1%. Thus, polypropylene fiber has a greater impact on the fracture properties of concrete than basalt fibers.

The aspect ratio of polypropylene fiber is relatively small, and the load capacity of a single fiber is high (Liang et al., 2020). It can withstand the stress and energy released when the load is close to the instability load and the micro-cracks partially extend, and it will not be momentarily broken. Besides, it can also bear part of the stress after the micro-cracks penetrate the matrix, increase the fracture process unit cohesion of the zone and delay the time when micro cracks develop into macro cracks (Liang et al., 2019a). The elastic modulus of basalt fiber is relatively large, but its long diameter is relatively large, the load capacity of a single fiber is limited, and the bridging effect is small (Arslan, 2016). It is easily directly broken when the crack penetrates. Therefore, the instability toughness, cohesive toughness and fracture energy of concrete with basalt fiber to concrete are less improved than that with polypropylene fiber.

3.4.2 Mixed Fiber Specimens

Comparing all hybrid-fiber specimens of A5–A9 with a total content of 6 kg/m³ and A10–A12 with 9 kg/m³, the initial fracture toughness K_{Ic}^{ini} , unstable toughness K_{Ic}^{un} and measured cohesive toughness $K_{Ic,T}^C$ showed the same trend with the change in mixing ratio of polypropylene fiber and basalt fiber. Specimens A6 and A10 with the mass ratio of CF to BF is 2:1 have the largest increase in the same content group. Compared with specimen A1, the K_{Ic}^{ini} , K_{Ic}^{un} and fracture energy G_f of specimen A6 with the same total content increased by 7.0%, 9.8% and 25.6%, respectively. Specimen A12 increased by 11.8%, 9.3% and 18.1%, respectively, compared to specimen A2 with the same total content. Thus, the mixing of polypropylene fiber and basalt fiber can produce a positive effect to simultaneously improve the initial fracture toughness, unstable toughness and fracture energy of concrete. Specimens A9 and A12 with a mass ratio of 1:4 have the smallest increase in the same content group. Compared to the 6-kg/m³ specimen A1, K_{Ic}^{un} and G_f of specimen A9 with the same total content decreased by 7.2% and 34.1%. Compared to the 9-kg/m³ specimen A2, K_{Ic}^{un} and G_f of specimen A12 with the same total content decreased by 0.3% and 9.0%. This means that the improper mixing ratio of polypropylene fiber and basalt fiber produced a negative effect and prevented the two fibers from functioning.

Different blending ratios have different effects on the increase in fracture energy of concrete. In specimens A5–A9 with a total admixture of 6 kg/m³, the increase in fracture energy of the mixed fiber concrete is arranged from high to low as 2:1 > 4:1 > 1:1 > 1:2 > 1:4 (CF:BF). In

specimens A10–A12 with a total content of 9 kg/m³, the increase in fracture energy of mixed fiber concrete is arranged from high to low as 2:1 > 1:1 > 1:2 (CF:BF). Specimens A6 and A10 with mass ratio of CF to BF is 2:1 have the largest fracture energy in the same group. In addition, the increase in K_{Ic}^{un} of specimens A5–A9 with a total content of 6 kg/m³ was 11.8–32.2%, and the increase in G_f was 114.5–309.2%. Meanwhile, the increase in K_{Ic}^{un} of specimens A10–A12 with a total content of 9 kg/m³ was 26.5–38.7%, and the increase in G_f was 231.5–330.2%. Thus, the total blending amount of 9 kg/m³ had a better effect than 6 kg/m³.

The polypropylene fiber in the hybrid-fiber-reinforced concrete can reduce the crack length, and the basalt fiber can suppress the generation of micro-cracks. These two fibers work together to reduce the probability of micro-crack interpenetrating (Deng et al., 2020a). The effect of polypropylene fiber on the fracture toughness of concrete is more significant. When the proportion of polypropylene fiber begins to decrease, the reduction of polypropylene fiber decreases, and the effect of fiber mixing is greater than that of a small amount of polypropylene fiber (Liang et al. 2019c). Therefore, when the mixing ratio of polypropylene fiber and basalt fiber is greater than 2:1, the instability toughness of the hybrid-fiber concrete increases with the increase in proportion of polypropylene fiber. When the mixing ratio of polypropylene fiber and basalt fiber is less than 2:1, the polypropylene fiber reduction is too large, and the fiber mixing effect is not sufficient to offset the impact of the coarse polypropylene fiber reduction on the fracture toughness of the concrete, so the unstable toughness of hybrid-fiber concrete will decrease with the decrease in proportion of polypropylene fiber content.

3.5 Parameter Fitting of the Bilinear Softening Constitutive Curve of Hybrid-Fiber Concrete

The softening constitutive curve of concrete can reveal the change law of the cohesive force of concrete in the fracture process area, including linear and nonlinear types. The current research shows that the bilinear physical meaning is clear, which is close to the actual fracture and softening of concrete, and it is convenient for practical engineering application (Xu, 1999). Therefore, in this paper, the bilinear softening constitutive curve is used to calculate the theoretical cohesive toughness of each group of specimens, and the curve form is shown in Fig. 12. Compared with the measured cohesive toughness, the bilinear softening constitutive curve is consistent with the hybrid-fiber concrete.

In the bilinear softening constitutive curve, ordinate σ is the cohesive stress, abscissa w is the crack opening displacement in the fracture process area, and (w_s, σ_s) is the

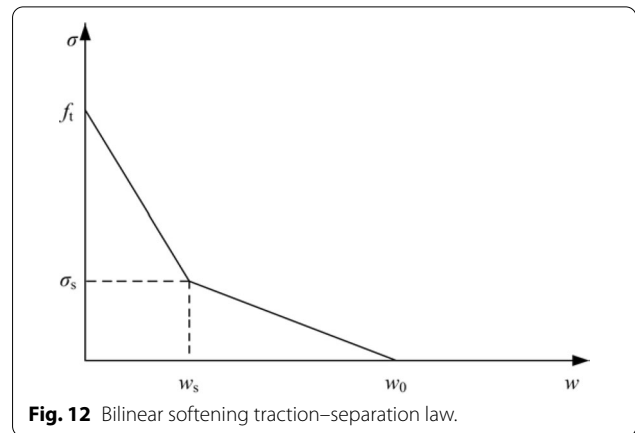


Fig. 12 Bilinear softening traction–separation law.

turning point coordinate. The values of σ_s , w_s and w_0 are different, and the form of the curve is also different.

The classic bilinear softening constitutive curves are shown below:

1. Peterson bilinear softening constitutive curve (Peterson, 1981):

$$\begin{cases} \sigma_s = f_t/3 \\ w_s = 0.8G_f/f_t, \\ w_0 = 3.6G_f/f_t \end{cases} \quad (1)$$

where G_f is the measured concrete fracture energy; f_t is the cube splitting tensile strength.

2. CEB-FIP Model Code 1990 bilinear softening constitutive curve (CEB-FIP, 1990):

$$\begin{cases} \sigma_s = 0.15f_t \\ w_s = 2G_f/f_t - 0.15w_0, \\ w_0 = \alpha_f G_f/f_t \end{cases} \quad (2)$$

where α_f is the parameter related to the maximum particle size d_{max} of the aggregate.

3. Bilinear softening constitutive curve proposed by Reinhardt and Xu (1999):

$$\begin{cases} \sigma_s = \frac{f_t}{\alpha_f} (2 - f_t w_s / G_f) \\ w_s = CTOD_C \\ w_0 = \alpha_f G_f / f_t \\ \alpha_f = \lambda - d_{max} / 8 \end{cases} \quad (3)$$

where $CTOD_c$ is the opening displacement of the virtual crack tip; λ is the correction parameter related to the deformation characteristics of concrete, whose value is 5–10.

Table 4 Comparison of $K_{Ic,T}^C$ and $K_{Ic,E}^C$ (MPa m^{1/2}).

Specimen	$K_{Ic,T}^C$	$K_{Ic,E}^C$ (Peterson)	$K_{Ic,E}^C$ (CEB-FIP)	$K_{Ic,E}^C$ (Xu and Reinhardt)					
				$\lambda=5$	$\lambda=6$	$\lambda=7$	$\lambda=8$	$\lambda=9$	$\lambda=10$
A0	0.440	0.303	0.277	0.462	0.370	0.335	0.316	0.304	0.296
	0.440	0.318	0.290	0.483	0.387	0.351	0.331	0.319	0.311
	0.443	0.310	0.283	0.475	0.380	0.343	0.324	0.312	0.304
T		0.051	0.075	0.003	0.012	0.029	0.042	0.050	0.057
A1	0.639	0.435	0.396	0.688	0.544	0.489	0.460	0.441	0.429
	0.683	0.416	0.379	0.654	0.518	0.466	0.439	0.421	0.410
	0.694	0.441	0.402	0.696	0.551	0.495	0.465	0.447	0.435
T		0.176	0.237	0.003	0.056	0.109	0.144	0.168	0.186
A2	0.734	0.449	0.409	0.710	0.561	0.504	0.474	0.455	0.443
	0.682	0.471	0.428	0.746	0.589	0.529	0.497	0.477	0.464
	0.697	0.457	0.335	0.723	0.571	0.513	0.482	0.463	0.450
T		0.183	0.301	0.005	0.054	0.110	0.148	0.174	0.193
A3	0.489	0.337	0.308	0.521	0.415	0.375	0.353	0.340	0.331
	0.435	0.338	0.308	0.518	0.414	0.374	0.353	0.340	0.331
	0.473	0.392	0.357	0.604	0.482	0.435	0.410	0.394	0.384
T		0.039	0.062	0.025	0.006	0.018	0.029	0.037	0.044
A4	0.475	0.356	0.325	0.548	0.437	0.395	0.372	0.358	0.349
	0.484	0.372	0.340	0.578	0.460	0.415	0.391	0.376	0.366
	0.476	0.363	0.331	0.563	0.448	0.404	0.381	0.366	0.356
T		0.040	0.065	0.022	0.003	0.016	0.028	0.037	0.044
A5	0.710	0.438	0.399	0.694	0.549	0.493	0.463	0.445	0.433
	0.692	0.470	0.427	0.746	0.589	0.528	0.496	0.476	0.463
	0.685	0.457	0.416	0.723	0.571	0.513	0.482	0.463	0.450
T		0.175	0.239	0.005	0.049	0.103	0.140	0.166	0.184
A6	0.727	0.476	0.433	0.756	0.597	0.536	0.503	0.483	0.470
	0.714	0.501	0.455	0.797	0.628	0.564	0.529	0.508	0.494
	0.718	0.492	0.447	0.782	0.617	0.553	0.520	0.499	0.485
T		0.160	0.227	0.012	0.035	0.086	0.124	0.150	0.169
A7	0.637	0.435	0.395	0.688	0.544	0.488	0.459	0.441	0.428
	0.625	0.420	0.383	0.664	0.525	0.472	0.444	0.426	0.414
	0.631	0.417	0.380	0.659	0.522	0.468	0.440	0.423	0.411
T		0.128	0.180	0.005	0.030	0.072	0.101	0.121	0.136
A8	0.502	0.384	0.350	0.603	0.478	0.430	0.405	0.389	0.378
	0.471	0.383	0.349	0.601	0.477	0.429	0.403	0.388	0.377
	0.491	0.361	0.329	0.565	0.449	0.404	0.380	0.366	0.356
T		0.023	0.047	0.077	0.001	0.004	0.012	0.020	0.026
A9	0.446	0.334	0.304	0.514	0.410	0.370	0.349	0.336	0.327
	0.455	0.345	0.315	0.536	0.427	0.385	0.362	0.349	0.339
	0.454	0.368	0.335	0.576	0.457	0.412	0.387	0.372	0.362
T		0.032	0.054	0.026	0.002	0.012	0.022	0.030	0.036
A10	0.745	0.518	0.471	0.822	0.649	0.582	0.547	0.525	0.510
	0.745	0.525	0.477	0.833	0.657	0.589	0.554	0.531	0.516
	0.713	0.524	0.476	0.832	0.656	0.589	0.553	0.531	0.516
T		0.136	0.204	0.028	0.020	0.066	0.102	0.127	0.146
A11	0.674	0.514	0.467	0.816	0.644	0.577	0.542	0.521	0.506
	0.660	0.497	0.452	0.787	0.622	0.558	0.525	0.504	0.490
	0.691	0.511	0.465	0.812	0.641	0.575	0.540	0.518	0.504
T		0.085	0.138	0.051	0.005	0.033	0.059	0.078	0.093

Table 4 (continued)

Specimen	$K_{Ic,T}^C$	$K_{Ic,E}^C$ (Peterson)	$K_{Ic,E}^C$ (CEB-FIP)	$K_{Ic,E}^C$ (Xu and Reinhardt)					
				$\lambda = 5$	$\lambda = 6$	$\lambda = 7$	$\lambda = 8$	$\lambda = 9$	$\lambda = 10$
A12	0.657	0.454	0.413	0.714	0.565	0.508	0.478	0.459	0.446
	0.652	0.463	0.421	0.727	0.576	0.518	0.487	0.468	0.455
T		0.018	0.038	0.055	0.001	0.004	0.010	0.017	0.021

One of the test specimens in the A12 group failed to obtain the test data due to errors in the test operation, so the A12 group only had two sets of data.

The calculation of the bilinear softening constitutive curves of each theory is summarized, and the calculation results are shown in Table 4.

In Table 4, the cumulative square sum T rarely exceeds 0.2, which represents the difference between theoretical cohesive toughness $K_{Ic,E}^C$ and measured cohesive toughness $K_{Ic,T}^C$ calculated by different softening constitutive curves for each group of test specimens; hence, the double-line softening constitutive curve is highly consistent with the actual softening stress distribution. It is reasonable to use the double-line softening constitutive curve to describe the fracture toughness law of plastic steel-basalt fiber concrete. The calculated values of Peterson's softening constitutive curve (Peterson, 1981) and softening constitutive curve recommended by the European standard CEB-FIP Model Code (CEB-FIP, 1990) are within the calculated value of the softening constitutive curve improved by Xu and Reinhardt. The reason is that the improved softening constituency of Reinhardt and Xu (1999) introduces correction parameter λ , which expands the value range of σ_s , w_s and other parameters, and improves the adaptability to the stress distribution of different concrete specimens. Parameters of the bilinear

softening curve of each fiber concrete specimen are shown in Table 5.

According to cumulative square sum T , the theoretical cohesive toughness $K_{Ic,E}^C$ obtained by the softening curves of Xu and Reinhardt is the closest to the measured cohesive toughness $K_{Ic,T}^C$. For plain concrete, the best value for λ is 5. When the total admixture is 3-kg/m³ and 6-kg/m³ single-admixed basalt fiber concrete, the best value for λ is 6. When the total admixture is 6-kg/m³ and 9-kg/m³ single-mixed polypropylene-fiber-reinforced concrete, it is appropriate to choose λ as 5. Thus, the effect of the total admixture on the softening curve of single-fiber concrete is not obvious. For hybrid-fiber concrete, the total fiber content and mixing ratio have a greater impact on the softening curve of concrete. The best value of λ is both 5 and 6: the value is 5 when the polypropylene fiber quality is relatively high, while it is 6 when the basalt fiber mass is relatively high.

4 Conclusions

The effect of hybrid fibers on the fracture toughness of concrete has been fully investigated by the three-point bending test of notched beams and acoustic emission technology with the double-K fracture theory of concrete. Some major conclusions may be summarized as follows:

1. Increasing the amount of fiber will weaken the workability of the mixture, which the optimum content of coarse polypropylene is 6 kg/m³ and basalt fiber is 3 kg/m³. In addition, coarse polypropylene fiber has a greater effect on the rheological properties of the concrete mixture than basalt fiber.
2. Increasing the content of fiber will not continue to significantly increase the fracture toughness of the concrete. The fracture toughness parameters of specimen A1 of 6 kg/m³ and A2 of 9 kg/m³ with coarse polypropylene fiber, and the specimen A3 of 3 kg/m³ and A4 of 6 kg/m³ with basalt fiber are relatively close.
3. Incorporation of fibers improves the fracture toughness parameters of concrete, but different fibers have

Table 5 Parameters of bilinear softening curve of hybrid-fiber concrete.

Specimen	λ	f_t (MPa)	σ_s (MPa)	w_s (mm)	w_0 (mm)
A0	5	3.19	4.58	0.009	0.056
A1	5	3.80	5.76	0.013	0.152
A2	5	3.86	5.85	0.014	0.168
A3	6	3.51	2.85	0.011	0.145
A4	6	3.60	2.96	0.011	0.169
A5	5	3.87	5.90	0.014	0.180
A6	5	3.96	6.23	0.015	0.183
A7	5	3.64	5.53	0.013	0.169
A8	6	3.54	2.97	0.012	0.239
A9	6	3.42	2.83	0.011	0.176
A10	6	4.15	3.94	0.016	0.331
A11	6	4.08	3.43	0.015	0.316
A12	6	3.92	2.93	0.015	0.312

different lifting ranges for different fracture parameters. The polypropylene fiber has a larger increase in unstable toughness, and the increase in initial fracture toughness of basalt fiber is greater.

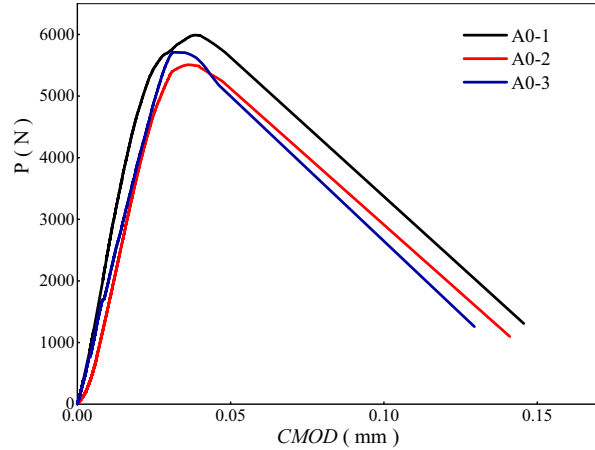
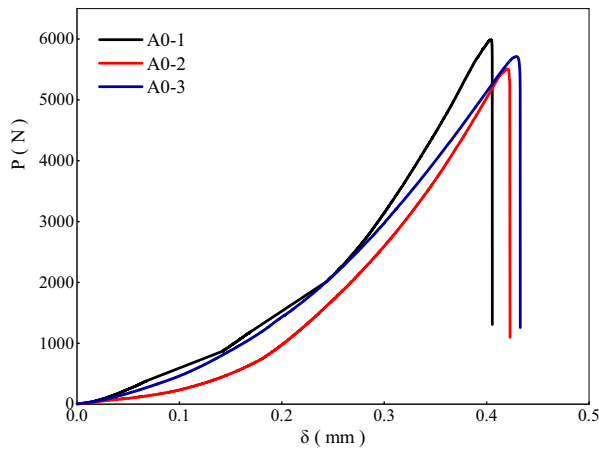
4. The optimal masse ratio of the polypropylene–basalt fiber is 2:1. When the mixing ratio is greater than or equal to 1:1, the fracture parameter of the hybrid-fiber specimens is higher than that of the single-fiber blend specimen. When the blending ratio is less than or equal to 1:2, the fracture parameter of the hybrid-fiber specimens is lower than that of the single-fiber blending specimen.
5. The softening curves proposed by Xu and Reinhardt are most consistent with the test results. The best value of correction parameter λ is 5 for plain concrete

and single-polypropylene–fiber-reinforced concrete, while it is 6 for single-basalt fiber. For hybrid-fiber-reinforced concrete, λ is 5 and 6 when the polypropylene and basalt fiber masses are relatively high, respectively.

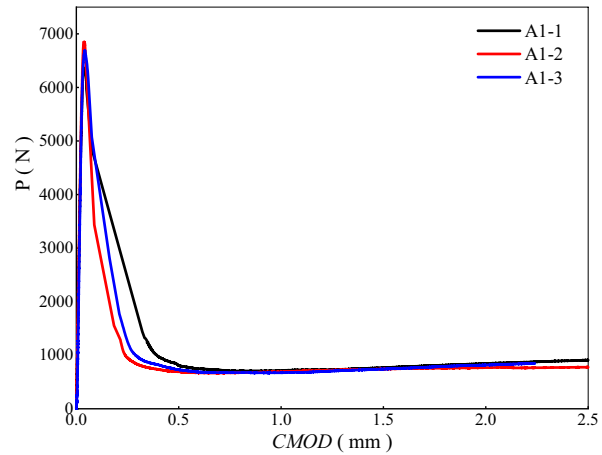
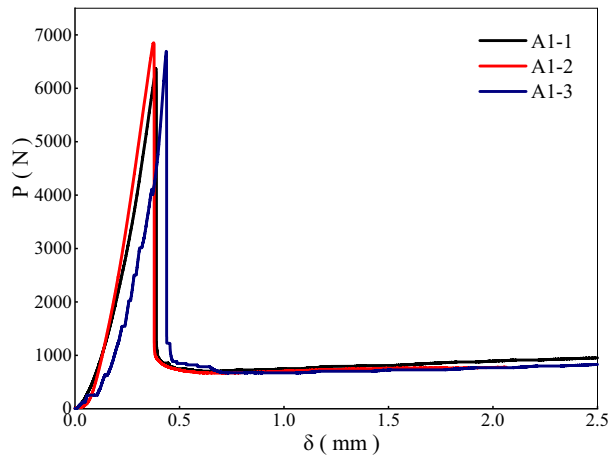
Appendices

Appendix 1: Load–Displacement Curves

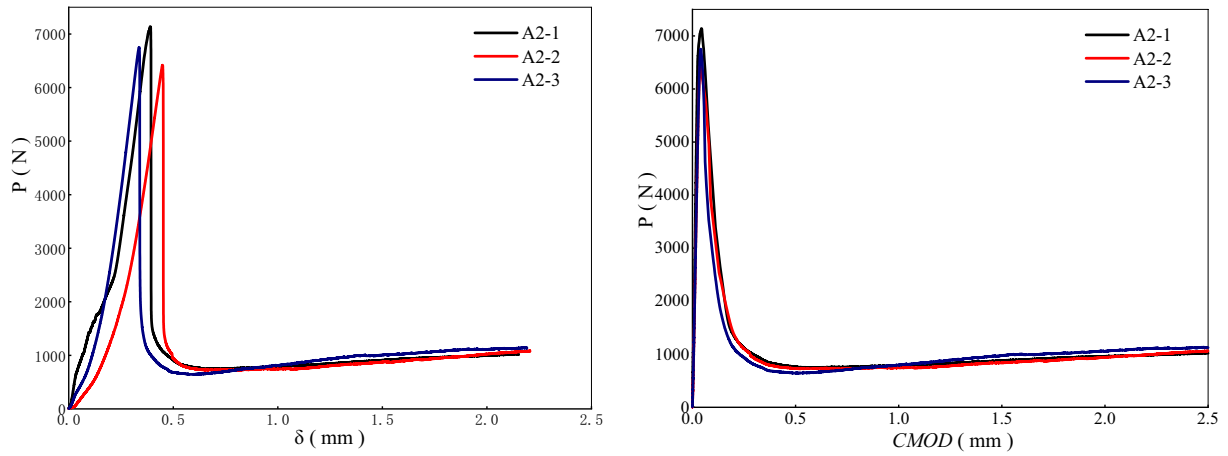
The load–displacement ($P-\delta$) curve and load–fracture opening-displacement ($P-CMOD$) curve of 13 sets of concrete specimens.



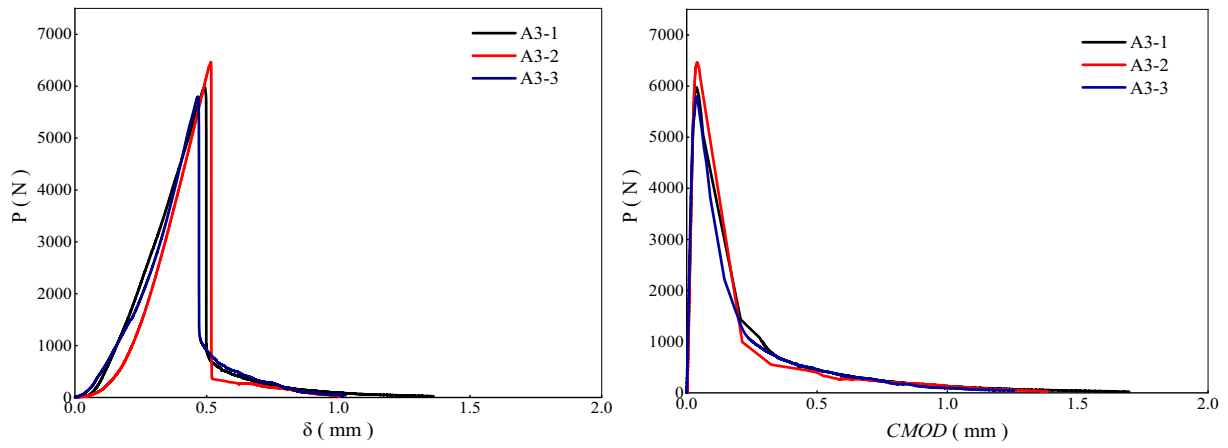
(1) specimen of A0



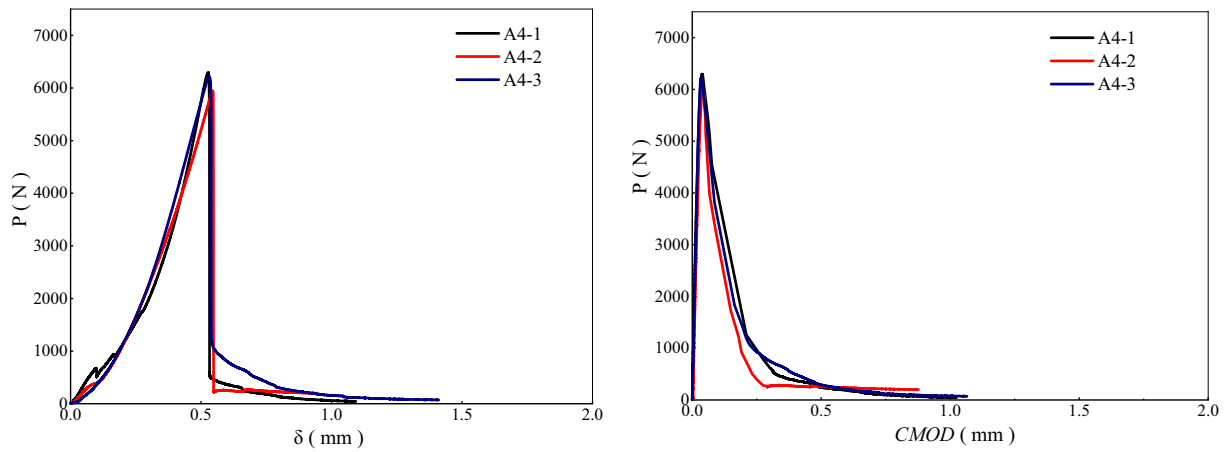
(2) specimen of A1



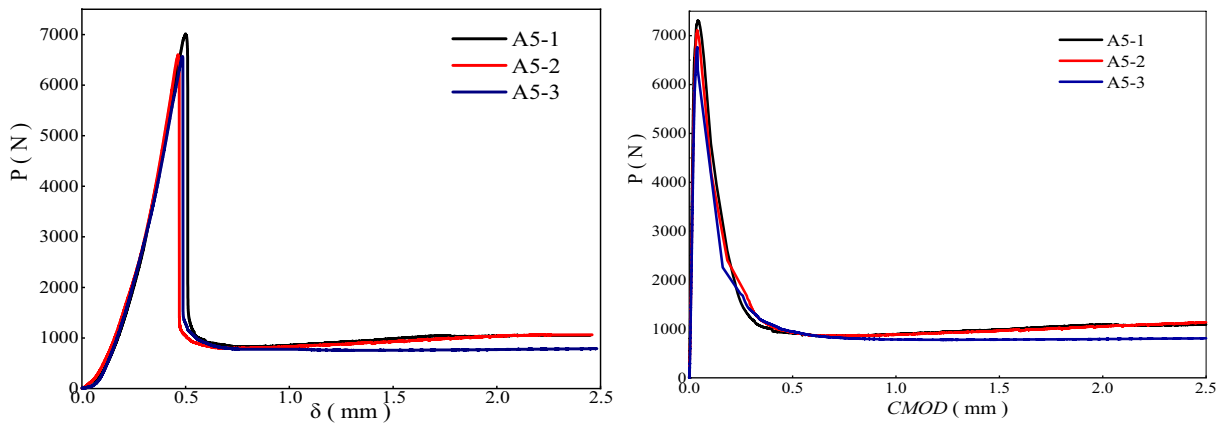
(3) specimen of A2



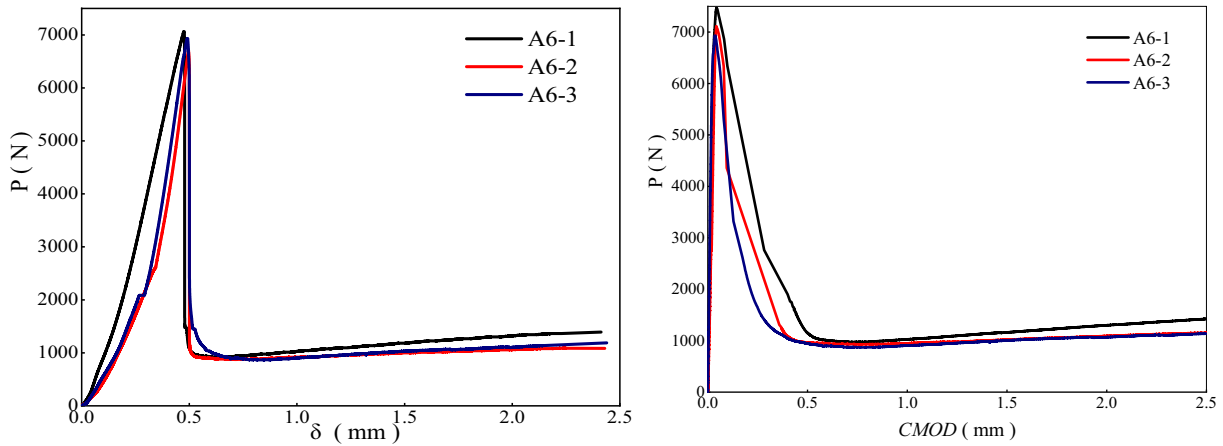
(4) specimen of A3



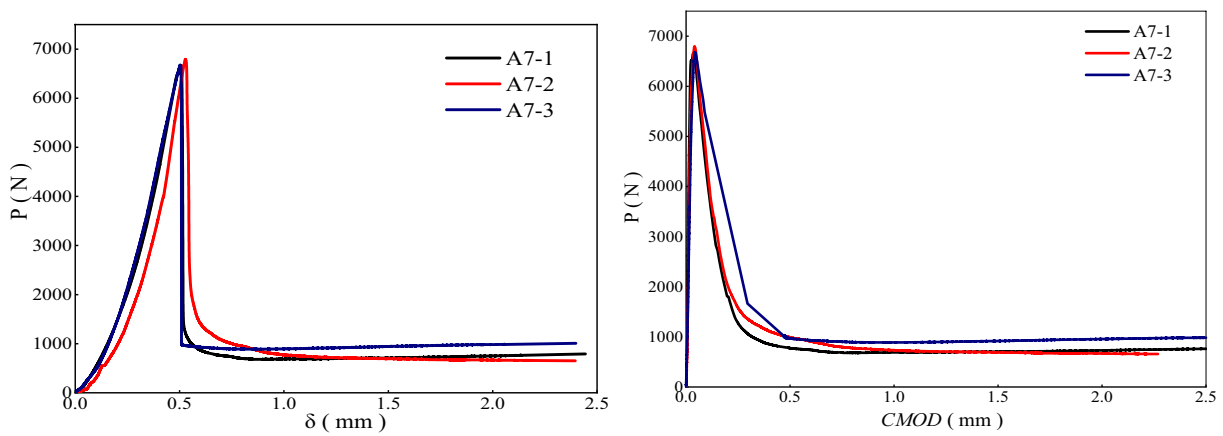
(5) specimen of A4



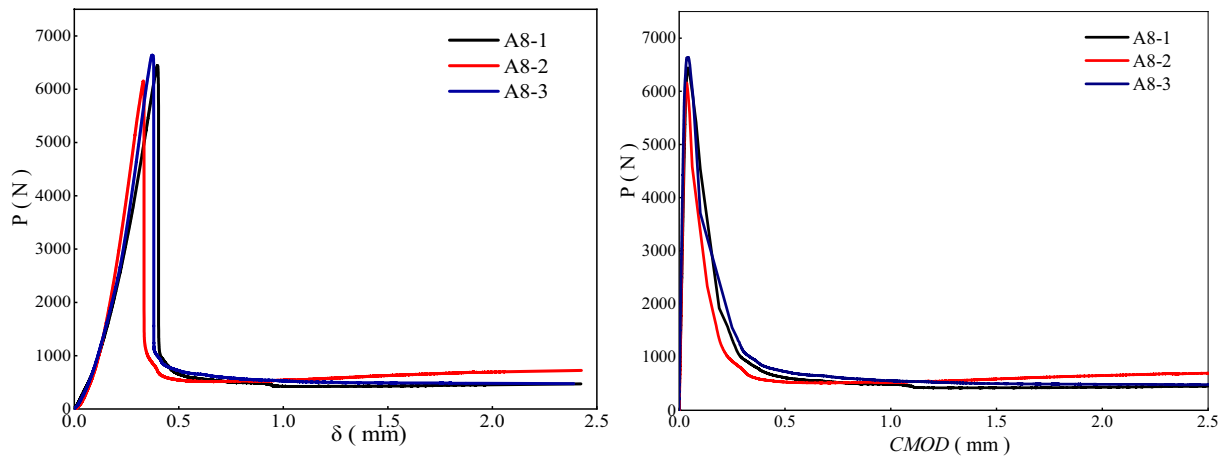
(6) specimen of A5



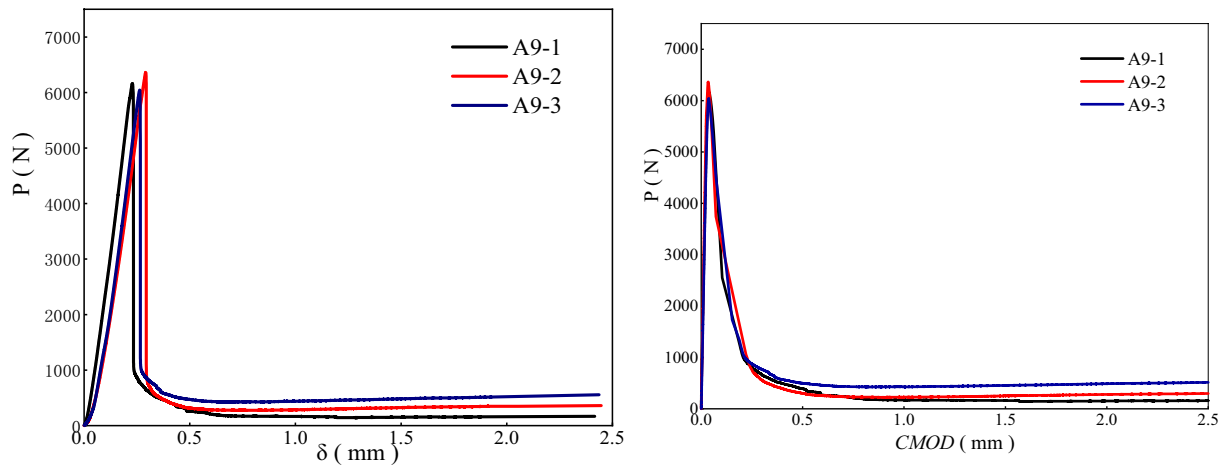
(7) specimen of A6



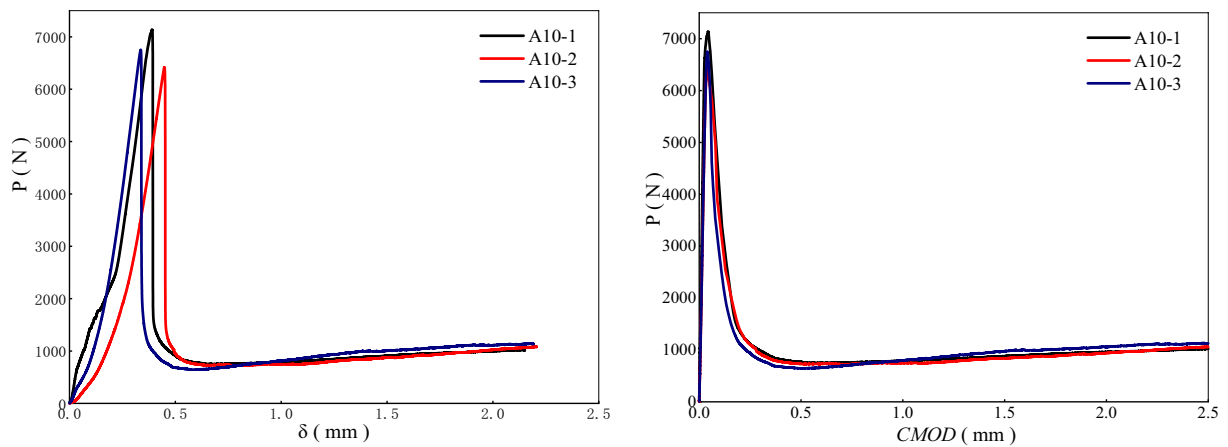
(8) specimen of A7



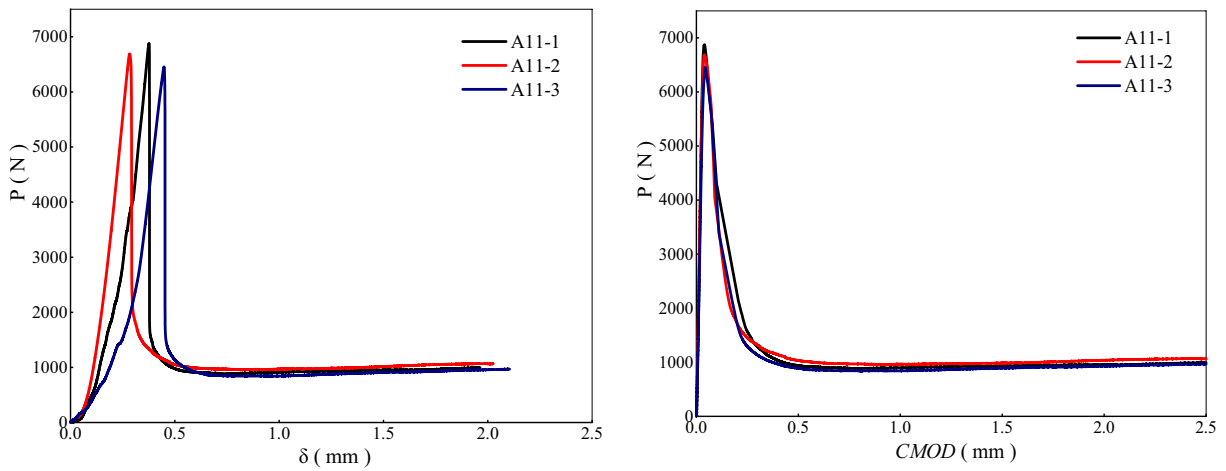
(9) specimen of A8



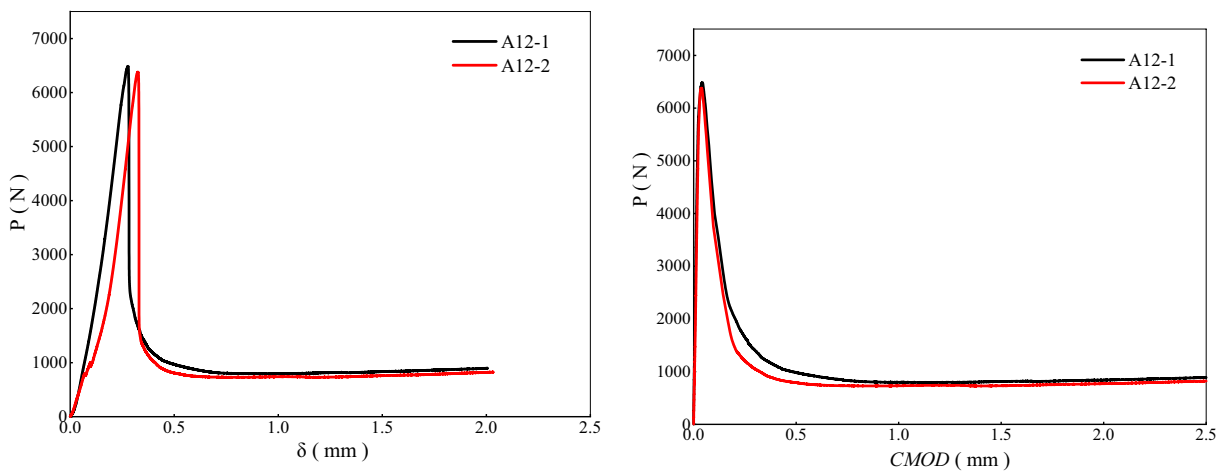
(10) specimen of A9



(11) specimen of A10



(12) specimen of A11



(13) specimen of A12

Note: One of the test specimens in the A12 group failed to obtain the test data due to errors in the test operation, so the A12 group only had two sets of data.

Appendix 2: Load–Displacement Parameters

Related load–displacement parameters of all specimens

Specimen		Initiation cracking load P_{ini} (N)	Instability load P_c (N)	Critical fracture process zone width $CTOD_c$ (mm)	Critical crack opening displacement $CMOD_c$ (mm)
A0	A0-1	4360	5489	0.0089	0.0354
	A0-2	4126	5308	0.0089	0.0351
	A0-3	4180	5413	0.0088	0.035
	Average	4204	5403	0.0089	0.0352
A1	A1-1	4984	6367	0.0124	0.0429
	A1-2	5411	6850	0.0127	0.045
	A1-3	5308	6692	0.0133	0.0454
	Average	5234	6636	0.0128	0.0444
A2	A2-1	5635	7135	0.0139	0.0485
	A2-2	5123	6518	0.0135	0.0445
	A2-3	5276	6752	0.0134	0.0463
	Average	5345	6802	0.0136	0.0464
A3	A3-1	4559	5974	0.0102	0.0373
	A3-1	5102	6465	0.0108	0.041
	A3-3	4464	5793	0.0117	0.0382
	Average	4595	6077	0.0109	0.0388
A4	A4-1	4893	6254	0.0108	0.0451
	A4-2	4991	6315	0.0115	0.0457
	A4-3	4826	6166	0.0109	0.0453
	Average	4903	6245	0.0110	0.0454
A5	A5-1	5606	7015	0.0135	0.0471
	A5-2	5217	6602	0.0139	0.0459
	A5-3	5162	6564	0.0133	0.0452
	Average	5328	6727	0.0136	0.0461
A6	A6-1	5614	7069	0.0141	0.0493
	A6-2	5352	6715	0.0147	0.0477
	A6-3	5546	6932	0.0145	0.0491
	Average	5504	6905	0.0144	0.0487
A7	A7-1	5377	6665	0.0137	0.0458
	A7-2	5515	6794	0.0134	0.0464
	A7-3	5377	6675	0.0131	0.0448
	Average	5425	6711	0.0134	0.0457
A8	A8-1	5079	6436	0.0120	0.0433
	A8-2	4881	6151	0.0114	0.0419
	A8-3	5270	6637	0.0115	0.0427
	Average	5076	6408	0.0117	0.0426
A9	A9-1	4778	6160	0.0101	0.0391
	A9-2	4990	6362	0.0109	0.0412
	A9-3	4715	6044	0.0112	0.0402
	Average	4828	6189	0.0107	0.0402
A10	A10-1	5985	7408	0.0161	0.0525
	A10-2	5723	7166	0.0159	0.0512
	A10-3	5676	7031	0.0155	0.0502
	Average	5795	7202	0.0159	0.0508
A11	A11-1	5585	6973	0.0154	0.0497
	A11-2	5602	6987	0.0148	0.0488
	A11-3	5386	6853	0.0150	0.0487
	Average	5524	6936	0.0150	0.0491

Specimen		Initiation cracking load P_{ini} (N)	Instability load P_c (N)	Critical fracture process zone width CTOD _c (mm)	Critical crack opening displacement CMOD _c (mm)
A12	A12-1	5485	6784	0.0154	0.046
	A12-2	5403	6679	0.0148	0.0458
	Average	5444	6732	0.0151	0.0459

One of the test specimens in the A12 group failed to obtain the test data due to errors in the test operation, so the A12 group only had two sets of data

Appendix 3: Fracture Toughness Parameters

The fracture toughness parameters K_{Ic}^{ini} , K_{Ic}^{un} , and K_{Ic}^C of all specimens

Specimen		a_c /mm	Δa /mm	K_{Ic}^{ini} /(MPa m ^{-0.5})	K_{Ic}^{un} /(MPa m ^{-0.5})	K_{Ic}^C /(MPa m ^{-0.5})
A0	A0-1	44.037	4.037	1.187	1.627	0.440
	A0-2	44.147	4.147	1.169	1.609	0.440
	A0-3	44.079	4.079	1.164	1.608	0.443
	Average	44.088	4.088	1.174	1.615	0.441
A1	A1-1	46.411	6.411	1.280	1.919	0.639
	A1-2	45.593	5.593	1.354	2.037	0.683
	A1-3	46.555	6.555	1.332	2.026	0.694
	Average	46.306	6.306	1.322	1.994	0.672
A2	A2-1	46.194	6.194	1.403	2.137	0.734
	A2-2	46.692	6.692	1.299	1.982	0.682
	A2-3	46.358	6.358	1.335	2.032	0.697
	Average	46.415	6.415	1.346	2.050	0.704
A3	A3-1	44.774	4.774	1.336	1.825	0.489
	A3-1	44.793	4.793	1.480	1.915	0.435
	A3-3	46.152	6.152	1.338	1.811	0.473
	Average	45.240	5.240	1.385	1.850	0.465
A4	A4-1	45.013	5.013	1.391	1.867	0.475
	A4-2	45.421	5.421	1.423	1.907	0.484
	A4-3	45.180	5.180	1.374	1.850	0.476
	Average	45.205	5.205	1.396	1.875	0.478
A5	A5-1	46.296	6.296	1.398	2.108	0.710
	A5-2	47.028	7.028	1.336	2.028	0.692
	A5-3	46.726	6.726	1.313	1.998	0.685
	Average	46.683	6.683	1.349	2.044	0.695
A6	A6-1	46.932	6.932	1.437	2.164	0.727
	A6-2	47.505	7.505	1.379	2.093	0.714
	A6-3	47.297	7.297	1.428	2.147	0.718
	Average	47.245	7.245	1.415	2.135	0.720
A7	A7-1	46.851	6.851	1.399	2.036	0.637
	A7-2	46.493	6.493	1.428	2.053	0.625
	A7-3	46.412	6.412	1.382	2.012	0.631
	Average	46.585	6.585	1.403	2.034	0.631

Specimen		a_c/mm	$\Delta a/mm$	$K_{Ic}^{ini}/(MPa\ m^{-0.5})$	$K_{Ic}^{un}/(MPa\ m^{-0.5})$	$K_{Ic}^c/(MPa\ m^{-0.5})$
A8	A8-1	45.870	5.870	1.407	1.909	0.502
	A8-2	45.826	5.826	1.351	1.822	0.471
	A8-3	45.292	5.292	1.444	1.935	0.491
	Average	45.663	5.663	1.401	1.889	0.488
A9	A9-1	44.905	4.905	1.330	1.776	0.446
	A9-2	45.192	5.192	1.395	1.850	0.455
	A9-3	45.786	5.786	1.334	1.788	0.454
	Average	45.294	5.294	1.353	1.805	0.452
A10	A10-1	47.345	7.345	1.552	2.297	0.745
	A10-2	47.496	7.496	1.487	2.233	0.745
	A10-3	47.483	7.483	1.477	2.190	0.713
	Average	47.442	7.442	1.505	2.240	0.734
A11	A11-1	47.451	7.451	1.495	2.169	0.674
	A11-2	47.073	7.073	1.489	2.149	0.660
	A11-3	47.396	7.396	1.437	2.129	0.691
	Average	47.307	7.307	1.474	2.149	0.675
A12	A12-1	46.520	6.520	1.495	2.052	0.557
	A12-2	46.730	6.730	1.481	2.033	0.552
	Average	46.625	6.625	1.488	2.043	0.554

One of the test specimens in the A12 group failed to obtain the test data due to errors in the test operation, so the A12 group only had two sets of data

The fracture energy of all specimens

Specimen		W_1 (N m)	W_2 (N m)	G_f (N/m)	Increase (%)
A0	A0-1	0.829	0.029	143.1	0
	A0-2	0.731	0.030	127.0	
	A0-3	0.906	0.031	156.1	
	Average	0.822	0.030	142.1	
A1	A1-1	2.668	0.181	474.9	225.7
	A1-2	2.555	0.150	450.7	
	A1-3	2.580	0.197	462.8	
	Average	2.601	0.176	462.8	
A2	A2-1	3.079	0.156	539.1	264.3
	A2-2	2.822	0.160	497.0	
	A2-3	2.941	0.159	516.7	
	Average	2.947	0.158	517.6	
A3	A3-1	1.379	0.099	246.3	58.9
	A3-2	1.227	0.073	216.7	
	A3-3	1.210	0.075	214.2	
	Average	1.272	0.082	225.7	
A4	A4-1	1.35	0.079	238.3	89.9
	A4-2	1.655	0.068	287.2	
	A4-3	1.602	0.102	284.0	
	Average	1.536	0.083	269.8	
A5	A5-1	3.430	0.153	597.1	292.1
	A5-2	3.277	0.164	573.5	
	A5-3	2.874	0.156	501.0	
	Average	3.194	0.158	557.2	

Specimen		W_1 (N m)	W_2 (N m)	G_f (N/m)	Increase (%)
A6	A6-1	3.43	0.747	597.1	309.2
	A6-2	3.277	0.778	573.5	
	A6-3	3.288	0.738	574.0	
	Average	3.332	0.754	581.5	
A7	A7-1	2.821	0.155	496.1	247.1
	A7-2	2.770	0.159	488.3	
	A7-3	2.822	0.149	495.2	
	Average	2.804	0.154	493.2	
A8	A8-1	2.062	0.144	367.7	164.8
	A8-2	2.145	0.149	382.4	
	A8-3	2.132	0.141	378.9	
	Average	2.113	0.145	376.3	
A9	A9-1	1.151	0.138	314.7	114.5
	A9-2	1.536	0.140	279.3	
	A9-3	1.781	0.140	320.2	
	Average	1.149	0.139	304.8	
A10	A10-1	3.702	0.173	645.9	330.2
	A10-2	3.229	0.152	593.6	
	A10-3	3.402	0.165	594.5	
	Average	3.444	0.163	611.3	
A11	A11-1	2.907	0.142	578.3	302.7
	A11-2	3.049	0.147	562.7	
	A11-3	2.881	0.153	575.6	
	Average	2.946	0.147	572.2	
A12	A12-1	2.819	0.145	494.1	231.4
	A12-2	2.540	0.147	447.8	
	Average	2.680	0.146	471.0	

One of the test specimens in the A12 group failed to obtain the test data due to errors in the test operation, so the A12 group only had two sets of data

Acknowledgements

Not applicable.

Authors' contributions

All authors contribute equally to this paper. Conceptualization: NL; writing—original draft: LR and ST; supervision: XL and ZZ; writing—review and editing: NL, ZD and RY. All authors have agreed to the published version of the manuscript. All authors read and approved the final manuscript.

Authors' information

Ninghui Liang is an Associate Professor in the School of Civil Engineering at Chongqing University. Lianxi Ren is a Master Student in the School of Civil Engineering at Chongqing University. Shuo Tian is a Master Student in the School of Civil Engineering at Chongqing University. Xinrong Liu is a Full Professor in the School of Civil Engineering at Chongqing University. Zuliang Zhong is an Associate Professor in the School of Civil Engineering at Chongqing University. Zhiyun Deng Ph.D. Student in the School of Civil Engineering at Chongqing University. Ru Yan is a Master Student in the School of Civil Engineering at Chongqing University.

Funding

This study was supported by the Natural Science Foundation of Chongqing, China (Grant No. cstc2018jcsx-mszdX0071) and the Graduate Scientific Research and Innovation Foundation of Chongqing, China (Grant No. CYS18025, No. CYS20027). This support is gratefully acknowledged.

Availability of data and materials

The data and materials had been included in the manuscript.

Declarations

Competing interests

The authors declare that they have no competing interests.

Author details

¹School of Civil Engineering, National Joint Engineering Research Center of Geohazards Prevention in the Reservoir Areas (Chongqing), and Key Laboratory of New Technology for Construction of Cities in Mountain Area (Chongqing University), Ministry of Education, Chongqing University, 400045 Chongqing, China. ²State Key Laboratory of Hydrosience and Engineering, Tsinghua University, 10084 Beijing, China. ³School of Civil Engineering, National Joint Engineering Research Center of Geohazards Prevention in the Reservoir Areas (Chongqing), and Key Laboratory of New Technology for Construction of Cities in Mountain Area (Chongqing University), Ministry of Education, Chongqing University, No. 83 Shabei Street, Shapingba District, 400045 Chongqing, China.

Received: 13 January 2021 Accepted: 9 July 2021

Published online: 04 August 2021

References

- Abdallah, S., Fan, M., & Zhou, X. (2017). Pull-out behaviour of hooked end steel fibres embedded in ultra-high performance mortar with various W/B ratios. *International Journal of Concrete Structures and Materials*, 11(2), 301–313. <https://doi.org/10.1007/s40069-017-0193-8>

- Abdallah, S., Fan, M., Zhou, X., & Le Geyt, S. (2016). Anchorage effects of various steel fibre architectures for concrete reinforcement. *International Journal of Concrete Structures and Materials*, 10(3), 325–335. <https://doi.org/10.1007/s40069-016-0148-5>
- Afroughsabet, V., & Ozbakkaloglu, T. (2015). Mechanical and durability properties of high-strength concrete containing steel and polypropylene fibers. *Construction and Building Materials*, 94, 73–82. <https://doi.org/10.1016/j.conbuildmat.2015.06.051>
- Arslan, M. E. (2016). Effect of basalt fibers on fracture energy and mechanical properties of HSC. *Computers and Concrete*, 17(4), 553–566.
- Ayub, T., Shafiq, N., & Nuruddin, M. F. (2014a). Effect of chopped basalt fibers on the mechanical properties and microstructure of high performance fiber reinforced concrete. *Advances in Materials Science and Engineering*. <https://doi.org/10.1155/2014/587686>
- Ayub, T., Shafiq, N., & Nuruddin, M. F. (2014b). Mechanical properties of high-performance concrete reinforced with basalt fibers. In M. S. Ali, M. Adnan, & M. Umer (Eds.), *Fourth international symposium on infrastructure engineering in developing countries* (pp. 131–139). Elsevier Science Bv.
- Banthia, N. (2005). Flexural response of hybrid fiber-reinforced cementitious composites. *Materials Journal*, 102(6), 382.
- Banthia, N., Majdzadeh, F., Wu, J., & Bindiganavile, V. (2014). Fiber synergy in hybrid fiber reinforced concrete (HyFRC) in flexure and direct shear. *Cement and Concrete Composites*, 48, 91–97. <https://doi.org/10.1016/j.cemconcomp.2013.10.018>
- Betterman, L. R., Ouyang, C., & Shah, S. P. (1995). Fiber–matrix interaction in microfiber-reinforced mortar. *Advanced Cement Based Materials*, 2(2), 53–61. [https://doi.org/10.1016/1065-7355\(95\)90025-X](https://doi.org/10.1016/1065-7355(95)90025-X)
- Branston, J., Das, S., Kenno, S. Y., & Taylor, C. (2016). Mechanical behaviour of basalt fibre reinforced concrete. *Construction and Building Materials*, 124, 878–886. <https://doi.org/10.1016/j.conbuildmat.2016.08.009>
- Buratti, N., & Mazzotti, C. (2015). Experimental tests on the effect of temperature on the long-term behaviour of macrosynthetic fibre reinforced concretes. *Construction and Building Materials*, 95, 133–142. <https://doi.org/10.1016/j.conbuildmat.2015.07.073>
- Buratti, N., Mazzotti, C., & Savoia, M. (2011). Post-cracking behaviour of steel and macro-synthetic fibre-reinforced concretes. *Construction and Building Materials*, 25(5), 2713–2722. <https://doi.org/10.1016/j.conbuildmat.2010.12.022>
- CEB-FIP. (1990). CEB-FIP model code 1990, first draft. *Ceb Bulletin Dinformation*, 195, 196.
- CECS-13:2009. (2009). Standard test methods for fiber reinforced concrete. *Chinese Association Standards of Engineering Construction Standardization*.
- Chi, Y., Xu, L. H., & Zhang, Y. Y. (2014). Experimental study on hybrid fiber-reinforced concrete subjected to uniaxial compression. *Journal of Materials in Civil Engineering*, 26(2), 211–218. [https://doi.org/10.1061/\(asce\)mt.1943-5533.0000764](https://doi.org/10.1061/(asce)mt.1943-5533.0000764)
- Das, C. S., Dey, T., Dandapat, R., Mukharjee, B. B., & Kumar, J. (2018). Performance evaluation of polypropylene fibre reinforced recycled aggregate concrete. *Construction and Building Materials*, 189, 649–659. <https://doi.org/10.1016/j.conbuildmat.2018.09.036>
- Deng, Z., Liu, X., Chen, P., de la Fuente, A., Zhou, X., Liang, N., Han, Y., & Du, L. (2020a). Basalt-polypropylene fiber reinforced concrete for durable and sustainable pipe production. Part 1: experimental program. *Structural Concrete*. <https://doi.org/10.1002/suco.202000759>
- Deng, Z., Liu, X., Yang, X., Liang, N., Yan, R., Chen, P., Miao, Q., & Xu, Y. (2020b). A study of tensile and compressive properties of hybrid basalt–polypropylene fiber-reinforced concrete under uniaxial loads. *Structural Concrete*. <https://doi.org/10.1002/suco.202000006>
- DL/T5332. (2005). *Technical specification for fiber reinforced concrete structures*. Electric Power Press of China.
- Fei, X., Bing, W., Luguang, S. (2018). Experimental study on the effect of polypropylene fiber on properties of stiff recycled concrete. *Journal of Yangzhou Polytechnic College*, 22(03), 27–29+37. (in Chinese)
- Fu, Q., Niu, D., Li, D., Wang, Y., Zhang, J., & Huang, D. (2018a). Impact characterization and modelling of basalt-polypropylene fiber-reinforced concrete containing mineral admixtures. *Cement & Concrete Composites*, 93, 246–259. <https://doi.org/10.1016/j.cemconcomp.2018.07.019>
- Fu, Q., Niu, D., Zhang, J., Huang, D., & Hong, M. (2018b). Impact response of concrete reinforced with hybrid basalt-polypropylene fibers. *Powder Technology*, 326, 411–424. <https://doi.org/10.1016/j.powtec.2017.12.022>
- GB/T-50080. (2016). *Standard for test method of performance on ordinary fresh concrete*. Ministry of Construction of the People's Republic of China.
- Guler, S., Yavuz, D., Korkut, F., & Ashour, A. (2019). Strength prediction models for steel, synthetic, and hybrid fiber reinforced concretes. *Structural Concrete*, 20(1), 428–445. <https://doi.org/10.1002/suco.201800088>
- Jalasutram, S., Sahoo, D. R., & Matsagar, V. (2017). Experimental investigation of the mechanical properties of basalt fiber-reinforced concrete. *Structural Concrete*, 18(2), 292–302. <https://doi.org/10.1002/suco.201500216>
- JDJ-52 2006. (2006). *Standard for technical requirements and test method of sand crushed stone (or gravel) for ordinary concrete*. China Architecture & Building Press.
- Jiang, C., Fan, K., Wu, F., & Chen, D. (2014). Experimental study on the mechanical properties and microstructure of chopped basalt fibre reinforced concrete. *Materials & Design*, 58, 187–193. <https://doi.org/10.1016/j.matdes.2014.01.056>
- Jiang, C., Huang, S., Zhu, Y., Lin, Y., & Chen, D. (2016). Effect of polypropylene and basalt fiber on the behavior of mortars for repair applications. *Advances in Materials Science and Engineering*. <https://doi.org/10.1155/2016/5927609>
- Kasagani, H., & Rao, C. B. K. (2018). Effect of graded fibers on stress strain behaviour of glass fiber reinforced concrete in tension. *Construction and Building Materials*, 183, 592–604. <https://doi.org/10.1016/j.conbuildmat.2018.06.193>
- Komlos, K., Babal, B., & Nurnbergerova, T. (1995). Hybrid fibre-reinforced concrete under repeated loading. *Nuclear Engineering and Design*, 156(1–2), 195–200. [https://doi.org/10.1016/0029-5493\(94\)00945-u](https://doi.org/10.1016/0029-5493(94)00945-u)
- Liang, N., Hu, Y., Zhong, Y., & Liu, X. (2019b). Study on pore structure and frost resistance of multi-scale polypropylene fiber reinforced concrete. *Journal of Chongqing University (Natural Science Edition)*, 42(11), 38–46. <https://doi.org/10.11835/j.issn.1000-582X.2019.11.005>
- Liang, N., Cao, G., Liu, X., Dai, J., & Miao, Q. (2020). Study on bridging stress of polypropylene fiber based on three-point bending test. *Materials Reports*, 34(02), 2153–2158. in Chinese.
- Liang, N., Dai, J., Liu, X., & Zhong, Z. (2019a). Experimental study on the fracture toughness of concrete reinforced with multi-size polypropylene fibres. *Magazine of Concrete Research*, 71(9), 468–475. <https://doi.org/10.1680/jmacr.17.00474>
- Liang, N., Miao, Q., Liu, X., Dai, J., & Zhong, Z. (2019c). Determination of fracture toughness and softening traction-separation law of polypropylene fiber reinforced concrete. *Journal of Jilin University (Engineering and Technology Edition)*, 49(04), 1144–1152. <https://doi.org/10.13229/j.cnki.jdxbgxb.20180020> in Chinese.
- Liu, W. (2013). Experimental research on mechanical properties and strengthening mechanisms of steel and basalt hybrid fiber-reinforced cement mortar. *Concrete*, 12, 125–128. in Chinese.
- Mudadu, A., Tiberti, G., Germano, F., Plizzari, G. A., & Morbi, A. (2018). The effect of fiber orientation on the post-cracking behavior of steel fiber reinforced concrete under bending and uniaxial tensile tests. *Cement and Concrete Composites*, 93, 274–288. <https://doi.org/10.1016/j.cemconcomp.2018.07.012>
- Nataraja, M. C., Dhang, N., & Gupta, A. P. (1999). Stress–strain curves for steel–fiber reinforced concrete under compression. *Cement and Concrete Composites*, 21(5–6), 383–390. [https://doi.org/10.1016/S0958-9465\(99\)00021-9](https://doi.org/10.1016/S0958-9465(99)00021-9)
- Niu, J., Zuo, F., Wang, J., & Xie, C. (2018). Freeze–thaw damage model of plastic–steel fiber reinforced lightweight aggregate concrete. *Journal of Building Materials*, 21(02), 235–240. in Chinese.
- Peterson, P. (1981). *Crack growth and development of fracture zone in plane concrete and similar materials*. Division of Building Materials.
- Reinhardt, H. W., & Xu, S. L. (1999). Crack extension resistance based on the cohesive force in concrete. *Engineering Fracture Mechanics*, 64(5), 563–587. [https://doi.org/10.1016/S0013-7944\(99\)00080-6](https://doi.org/10.1016/S0013-7944(99)00080-6)
- Smazewski, P. (2018a). Flexural toughness of high-performance concrete with basalt and polypropylene short fibres. *Advances in Civil Engineering*, 2018, 1–8. <https://doi.org/10.1155/2018/5024353>
- Smazewski, P. (2018b). Flexural toughness of high-performance concrete with basalt and polypropylene short fibres. *Advances in Civil Engineering*. <https://doi.org/10.1155/2018/5024353>
- Smazewski, P. (2019). Influence of basalt–polypropylene fibres on fracture properties of high performance concrete. *Composite Structures*, 209, 23–33. <https://doi.org/10.1016/j.compstruct.2018.10.070>

- Smarzewski, P. (2020). Comparative fracture properties of four fibre reinforced high performance cementitious composites. *Materials*. <https://doi.org/10.3390/ma13112612>
- Smarzewski, P., & D'Aniello, M. (2018). Flexural toughness of high-performance concrete with basalt and polypropylene short fibres. *Advances in Civil Engineering*, 2018, 1–8.
- Soroushian, P., Elyamany, H., Tlili, A., & Ostowari, K. (1998). Mixed-mode fracture properties of concrete reinforced with low volume fractions of steel and polypropylene fibers. *Cement & Concrete Composites*, 20(1), 67–78. [https://doi.org/10.1016/s0958-9465\(97\)87390-8](https://doi.org/10.1016/s0958-9465(97)87390-8)
- Wang, D., Ju, Y., Shen, H., & Xu, L. (2019). Mechanical properties of high performance concrete reinforced with basalt fiber and polypropylene fiber. *Construction and Building Materials*, 197, 464–473. <https://doi.org/10.1016/j.conbuildmat.2018.11.181>
- Xia, D., Liu, X., Xia, G., & Zhou, B. (2013). Flexural toughness of high-performance hybrid fiber reinforced concrete. *Journal of Huazhong University of Science and Technology (Natural Science Edition)*, 41(06), 108–112. in Chinese.
- Xu, S. (1999). Determination of parameters in the bilinear, Reinhardt's and exponentially nonlinear softening curves and their physical meaning. *Werkstoffe und Werkstoffprüfung Im Bauwesen Hamburg, LibriBOD*, 01, 410–424.
- Zhang, H., Wang, L., Bai, L., Addae, M., & Neupane, A. (2019). Research on the impact response and model of hybrid basalt-macro synthetic polypropylene fiber reinforced concrete. *Construction and Building Materials*, 204, 303–316. <https://doi.org/10.1016/j.conbuildmat.2019.01.201>
- Zhu, H., Gao, D., & Wang, Z. (2010). Experimental study on fracture properties of hybrid fiber reinforced high-strength concrete. *Journal of Building Structures*, 31(01), 41–46. <https://doi.org/10.14006/j.jzjgxb.2010.01.002> in Chinese.
- Zieliński, K., & Olszewski, P. (2005). The impact of basaltic fibre on selected physical and mechanical properties of cement mortar. *Betonwerk Und Fertigteil Technik/Concrete Precasting Plant & Technology*, 71(3), 28–33.

Publisher's Note

Springer Nature remains neutral with regard to jurisdictional claims in published maps and institutional affiliations.

Submit your manuscript to a SpringerOpen[®] journal and benefit from:

- Convenient online submission
- Rigorous peer review
- Open access: articles freely available online
- High visibility within the field
- Retaining the copyright to your article

Submit your next manuscript at ► [springeropen.com](https://www.springeropen.com)
